Neurobiology of Disease 125 (2019) 31–44

Contents lists available at ScienceDirect

Neurobiology of Disease

journal homepage: www.elsevier.com/locate/ynbdi

A two-hit story: Seizures and genetic mutation interaction sets phenotype severity in *SCN1A* epilepsies

Ana Rita Salgueiro-Pereira[a], Fabrice Duprat[b], Paula A. Pousinha[a], Alexandre Loucif[b], Vincent Douchamps[d], Cristina Regondi[c], Marion Ayrault[b], Martine Eugie[a], Marion I. Stunault[a], Andrew Escayg[e], Romain Goutagny[d], Vadym Gnatkovsky[c], Carolina Frassoni[c], Hélène Marie[a], Ingrid Bethus[a,*,1], Massimo Mantegazza[b,*,1]

[a] *Université Côte d'Azur (UCA), CNRS UMR7275, Institute of Molecular and Cellular Pharmacology (IPMC), Team Physiopathology of Neuronal Circuits and Behavior, France*
[b] *Université Côte d'Azur (UCA), INSERM, CNRS UMR 7275, Institute of Molecular and Cellular Pharmacology (IPMC), Team Pathophysiology of Voltage-Gated Na^+ channels and of Neuronal Excitability, France*
[c] *U.O. Clinical and Experimental Epileptology, Fondazione IRCCS Istituto Neurologico Carlo Besta, Italy*
[d] *Université de Strasbourg, CNRS, LNCA, Strasbourg, France*
[e] *Department of Human Genetics, Emory University, Atlanta, GA, USA*

ARTICLE INFO

Keywords:
Dravet syndrome
GEFS+
Epileptogenesis
Precision medicine
Seizures
Remodeling
Autism
Cognition

ABSTRACT

SCN1A ($Na_V1.1$ sodium channel) mutations cause Dravet syndrome (DS) and GEFS+ (which is in general milder), and are risk factors in other epilepsies. Phenotypic variability limits precision medicine in epilepsy, and it is important to identify factors that set phenotype severity and their mechanisms. It is not yet clear whether *SCN1A* mutations are necessary for the development of severe phenotypes or just for promoting seizures. A relevant example is the pleiotropic R1648H mutation that can cause either mild GEFS+ or severe DS.

We used a R1648H knock-in mouse model (*Scn1a*$^{RH/+}$) with mild/asymptomatic phenotype to dissociate the effects of seizures and of the mutation *per se*. The induction of short repeated seizures, at the age of disease onset for *Scn1a* mouse models (P21), had no effect in WT mice, but transformed the mild/asymptomatic phenotype of *Scn1a*$^{RH/+}$ mice into a severe DS-like phenotype, including frequent spontaneous seizures and cognitive/behavioral deficits. In these mice, we found no major modifications in cytoarchitecture or neuronal death, but increased excitability of hippocampal granule cells, consistent with a pathological remodeling.

Therefore, we demonstrate for our model that an *SCN1A* mutation is a prerequisite for a long term deleterious effect of seizures on the brain, indicating a clear interaction between seizures and the mutation for the development of a severe phenotype generated by pathological remodeling. Applied to humans, this result suggests that genetic alterations, even if mild *per se*, may increase the risk of second hits to develop severe phenotypes.

1. Introduction

More than 1000 pathogenic mutations of *SCN1A*, the gene coding for the $Na_V1.1$ voltage-gated sodium channel, have been identified thus far (www.gzneurosci.com/*Scn1a*database) and can cause well defined epilepsies (Orsini et al., 2018), but genotype-phenotype correlation and selection of therapies are still challenging (Balestrini and Sisodiya, 2018). In fact, pleiotropy is often observed, with a single mutation that can induce a spectrum of phenotypes (from very mild to very severe, with sometimes incomplete penetrance), and we lack a holistic understanding of pathophysiological mechanisms and risk factors leading to severe phenotypes (Balestrini and Sisodiya, 2018; Symonds and Zuberi, 2018). This is an important issue for the prediction of outcome and the selection of therapies in genetic epilepsies, in particular in an era of high throughput sequencing-mediated identification of genetic variants that could potentially be exploited for precision medicine (Avanzini et al., 2018; Guerrini et al., 2014; Symonds and Zuberi, 2018). Yet, this approach is still limited in epilepsy, also because of an incomplete understanding of pleiotropy mechanisms (Balestrini and Sisodiya, 2018; Symonds and Zuberi, 2018). Thus, it is

* Corresponding authors.
E-mail addresses: bethus@ipmc.cnrs.fr (I. Bethus), mantegazza@ipmc.cnrs.fr (M. Mantegazza).
[1] Co-last and co-corresponding authors:

https://doi.org/10.1016/j.nbd.2019.01.006
Received 25 October 2018; Received in revised form 14 December 2018; Accepted 14 January 2019
Available online 17 January 2019
0969-9961/

important to identify factors that can modulate the effect of genetic variants in order to disclose risks for the development of severe phenotypes. It is often hypothesized that pleiotropy is generated by epistatic interactions between pathogenic variants and modifier genes (Symonds and Zuberi, 2018), but modifications of disease's features and progression can also be induced by interactions with environmental factors (Berkovic et al., 2006). Seizures are considered as an important factor for phenotype worsening in epilepsy, in particular in epileptic encephalopathies (EEs), in which epileptic activity is thought to strongly contribute to cognitive and behavioral impairments (Scheffer et al., 2017).

Mutations of *SCN1A* are relevant examples of these issues: they cause Dravet syndrome (DS) (Dravet, 2011), which has been classified as a severe EE, and genetic epilepsy with febrile seizures plus (GEFS +), which is milder but with a large phenotypic variability (*e.g.* about 3% of GEFS + patients develop DS) (Zhang et al., 2017). For instance, the R1648H mutation causes mild GEFS + in one family (Escayg et al., 2000), but DS in another family (Depienne et al., 2010); there are asymptomatic carriers in both families and germinal mosaicism has been excluded as the cause of phenotypic variability (Depienne et al., 2010). Moreover, *SCN1A* genetic variants are also risk factors for different types of common epilepsies, (Epi4K consortium and Epilepsy Phenome/Genome Project, 2017; EPICURE Consortium et al., 2012; ILAE, 2014; Kasperaviciute et al., 2013). Notably, there is an ongoing debate about the classification of DS: it has been proposed that phenotype severity depends on the type of *SCN1A* mutation and not on effects of epileptic activity as in EEs, consistent with the concept of pure channelopathy (Brunklaus et al., 2014; Gataullina and Dulac, 2017; Parihar and Ganesh, 2013) and with the definition of developmental encephalopathy (DE) (Scheffer et al., 2017).

Animal models of *Scn1a* epileptogenic mutations reproduce clinical phenotypes and have been instrumental to demonstrate that $Na_V1.1$ loss-of-function mutations cause hypoexcitability of GABAergic neurons leading to reduced GABAergic inhibition, which is the main initial seizure-triggering mechanism (Hedrich et al., 2014; Ogiwara et al., 2007; Yu et al., 2006). Notably, heterozygous *Scn1a*$^{+/-}$ mice carrying truncating mutations exhibit a severe phenotype in the C57BL/6J genetic background, but very mild phenotype in the 129 background (Ogiwara et al., 2007; Rubinstein et al., 2015; Yu et al., 2006). It has been proposed that $Na_V1.1$ dysfunctions induced by the mutation could be the direct cause of behavioral and cognitive deficits in mice, supporting the hypothesis that DS is a pure channelopathy and a DE, rather than an EE (Bender et al., 2013; Han et al., 2012). Challenging these results, a recent study has shown that, consistent with the EE concept, hyperthermic long seizures/*status epilepticus* can worsen the mild phenotype of *Scn1a* knock-in mice carrying the R1648H mutation (*Scn1a*$^{RH/+}$) (Dutton et al., 2017). However, early-life hyperthermic long seizures/*status epilepticus* can cause recurrent spontaneous seizures and cognitive/behavioral impairments also in wild type (WT) rodents, questioning its specific effect in models carrying genetic mutations (Baram et al., 1997; Dubé et al., 2009).

Thus, the causal role of the genetic mutation/variant in the development of severe phenotypes has not been clearly discriminated from that of seizures. In particular, it is not clear yet if the *Scn1a* mutation is necessary for the development of severe phenotypes or just for inducing sensitivity to seizure triggers. Moreover, the role of short seizures in the generation of severe EE-like phenotypes has never been investigated in animal models of *Scn1a* mutations. In this study, we addressed these two specific issues comparing the effects of short seizures induced, at the age of disease onset for *Scn1a* models, with hyperthermia in *Scn1a*$^{RH/+}$ mice or with the convulsant flurothyl in both *Scn1a*$^{RH/+}$ mice and WT littermates. Thus, we have clearly dissociated the effects of short seizures *per se* from that of seizures occurring in a mouse carrying a *Scn1a* mutation in an otherwise mild/asymptomatic genetic background.

2. Material and methods

See Supplementary material for more details on methods. Details on statistical comparisons, including values and statistical tests used are presented in the Supplementary material (Supplementary Statistics Tables).

2.1. Mice

We used heterozygous knock-in mice carrying the R1648H $Na_V1.1$ (*Scn1a*) mutation (*Scn1a*$^{RH/+}$) (Martin et al., 2010) and their WT littermates in a hybrid mixed 129P2/OlaHsd x C57BL/6J background (F1 generation 50–50% 129:B6). Animals were genotyped at postnatal day 7 (P7) as previously described (Martin et al., 2010). All experiments were performed according to policies on the care and use of laboratory animals of European Communities Council Directive (2010/63EU) and under the agreement number 04551.02 from the French Ministry of research.

2.2. Induction of short seizures

Seizures were induced by hyperthermia (SIH) or with Flurothyl (SIF) once a day for 10 days, starting at P21. For the SIH protocol, the animal was placed in a small incubator and the core temperature, controlled using a rectal probe, was increased 0.5 °C every 2 min as described previously. The animal was immediately removed from the incubator when a behavioral seizure occurred or a maximum temperature of 42.5 °C was reached. For the SIF procedure, liquid flurothyl (Bis 2,2,2-trifluoroethyl ether) was delivered using a syringe pump injector at a rate of 10 µl/min and allowed to volatilize within the chamber. The animal was removed from the chamber at the onset of a generalized tonic clonic seizure. The severity classification of seizures is detailed in the Supplementary material.

Six experimental groups were evaluated: WT, *Scn1a*$^{RH/+}$, WT-SIH, *Scn1a*$^{RH/+}$-SIH, WT-SIF and *Scn1a*$^{RH/+}$-SIF. We compared *Scn1a*$^{RH/+}$ control mice with WT littermates to evaluate the effect of the mutation *per se*. WT-SIH mice were used to evaluate the effect of hyperthermia *per se*. The *Scn1a*$^{RH/+}$-SIH group represented the effect of hyperthermia-induced seizures in mutant mice. WT-SIF mice were used to evaluate the effect of seizures *per se* and compare to seizures in the mutant *Scn1a*$^{RH/+}$-SIF mice.

Following the protocol of SIH and SIF, different cohorts of animals underwent: 1) synchronized video-electrocorticogram (video-ECoG) recordings from P34 to P90, or 2) behavioral analysis from P60 to P90, or 3) electrophysiological recordings in brain slices (P60), or 4) immunohistochemical profiling (P60) (done for SIH groups only).

2.3. Video-EcoG recordings

For continuous electrocorticogram, five stainless steel recording electrodes (Plastic One, USA) fixed with screws on the skull were implanted on mice at P32. After a recovering period from surgery, the animals were connected to the amplifier and acquisition system. Infrared video cameras were synchronized to the acquisition of the ECoG signal (filtered at 0.1-1 kHz bandpass and sampled at 2 kHz), allowing the recording of electrographic and behavioral seizures simultaneously. The mice were recorded for 7 weeks in regular windows of 3.5 days. The analyses performed on the video-ECoG signal (including GTC seizures, interictal spikes, longitudinal long-term spectral analysis and spectral analysis at P60) are detailed in the Supplementary material.

2.4. Behavioral analysis

Behavioral analysis was conducted from P60 to P90 (Fig. 1A and 5A). – **Open Field.** The apparatus consisted in a white and opaque quadratic arena *(40x40cm)* with an imaginary central area *(20x20cm)*. The mouse was placed in the center of the arena and allowed to explore

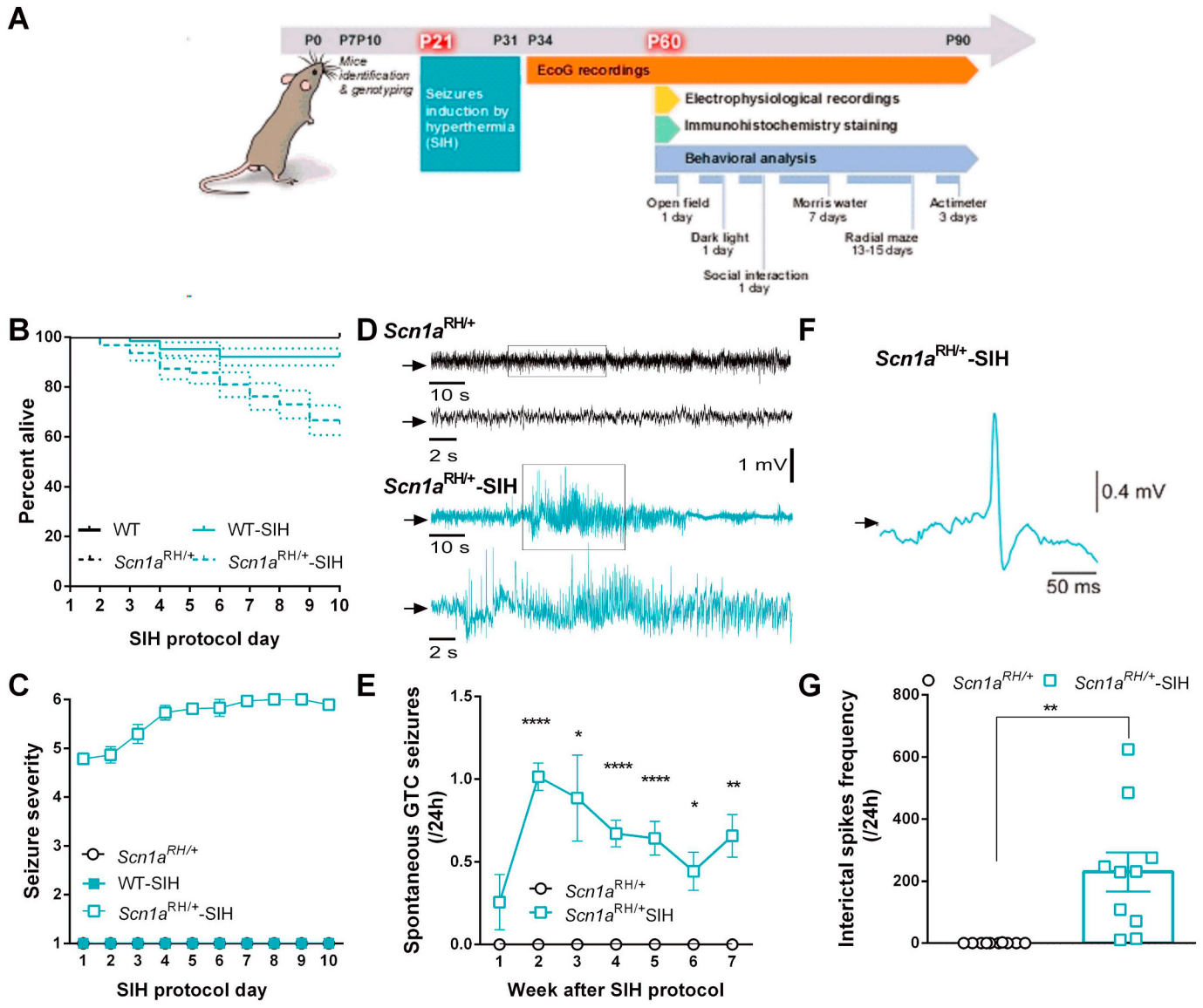

Fig. 1. The SIH protocol worsens the epileptic phenotype in *Scn1a*$^{RH/+}$ mutant mice.
A: Protocol timeline with the sequence of experiments from P7 to P90. All groups went through identification and genotyping, then the SIH protocol or control-SIH protocol (no hyperthermia but identical handling and exposure to apparatus) followed by either ECoG recordings, behavioral analysis, electrophysiological recordings or immunohistochemistry staining. SIH: 10 short daily seizures were induced starting at P21 (the age of disease onset in epileptic *Scn1a* mouse models and of plateau for the expression of $Na_V1.1$) (Dutton et al., 2017; Oakley et al., 2009; Ogiwara et al., 2007). B: Percentage of mice alive during the SIH or control protocol. WT (no hyperthermia) $N = 20$, *Scn1a*$^{RH/+}$ (no hyperthermia) N = 20, WT-SIH (hyperthermia that did not induce seizures) $N = 33$, *Scn1a*$^{RH/+}$-SIH (hyperthermia leading to seizure induction) $N = 63$. C: Characterization of seizure severity (see material and methods) for WT-SIH (N = 33), *Scn1a*$^{RH/+}$ (N = 20, data hidden by WT-SIH) and *Scn1a*$^{RH/+}$-SIH ($N = 47$). D: Representative ECoG traces recorded at P40, showing normal activity in a *Scn1a*$^{RH/+}$ mice and activity during a generalized tonic-clonic seizure in a *Scn1a*$^{RH/+}$-SIH mouse (including end of pre-ictal, ictal and initial post-ictal periods). The parts highlighted by the boxes, corresponding to ictal period in the *Scn1a*$^{RH/+}$-SIH recording, are displayed below the trace at a higher time resolution. The black arrows indicate 0 mV E: Average spontaneous GTC seizure frequency per 24 h observed for 7 weeks in *Scn1a*$^{RH/+}$ mice (N = 6) and *Scn1a*$^{RH/+}$-SIH mice ($N = 7$) from P34 to P90. F: Representative interictal spike recorded at P60 in a *Scn1a*$^{RH/+}$-SIH mouse; the black arrow indicates 0 mV. G: Interictal spikes' frequency (events/24 h) recorded at P60 in *Scn1a*$^{RH/+}$ ($N = 10$) and *Scn1a*$^{RH/+}$-SIH (N = 10) mice. See Supplementary Statistics Tables for details on statistics.

for 10 min. Locomotor activity, number of body rotations and thigmotaxis were measured as described in Supplementary material. – **Dark light.** The apparatus consisted of a white and black cage separated in two compartments (light and dark) by a partition, which had a small opening at the floor level. The mouse was placed in the center of the light compartment and allowed to explore for 5 min. – **Three-chamber test.** The apparatus consisted in a rectangular non-transparent plexiglass box (60 × 30 cm). Two dividing walls were made with clear plexiglass containing one circular opening each (4 cm diameter) to allow the mouse to assess to each chamber. The test consisted in a habituation phase to the empty apparatus, a sociability phase comparing interactions with an unfamiliar mouse and an empty chamber, and a social novelty phase comparing interactions with a familiar mouse and an unfamiliar mouse. – **Morris Water Maze.** The apparatus consisted in a circular tank (Ø 90 cm) filled with water (temperature 25 ± 1 °C) made opaque with the addition of 100 ml of white opacifier (Viewpoint, France). The test consisted in 3 phases: (1) Cue task training (2 days), (2) Spatial learning training (4 days) and (3) Long-term reference memory-probe test (1 day). An escape platform (Ø 8 cm) was submerged 1 cm below the water surface for the cue task training and the spatial learning training. – **8-arm Radial maze.** The apparatus consisted in a black plexiglass 8-arms radial maze

(Viewpoint, Lyon, France). The central platform (Ø 24 cm) and 8 arms (35 × 5 cm), which project radially outward, were elevated 8 cm above the floor. A metallic and weighted food cup was placed at the end of each arm. The procedure was divided in 2 phases: habituation (3 days) and training for a win-shift strategy in the choice between two arms (lasting until the criterion was reached). – **Actimeter.** Mice were placed in the actimeter (Imetronic Apparatus, Pessac, France) for 3 consecutive days (72 h).

2.5. Patch-clamp recordings

Acute transverse hippocampal slices (250 µm thick) were obtained from mice at P60. Current-clamp recordings were performed on CA1 pyramidal neurons or on dentate gyrus (DG) granule cells. To study the firing frequency in response to injected current, we first adjusted the membrane potential of CA1 pyramidal neurons at Vh = −70 mV and of DG granule cells at Vh = −60 mV and then injected pulses of increased intensity in steps of 20pA (from 0 to 400pA, 1 s duration). We compared input-output relationships, expressed as frequency of action potentials (AP) generated by depolarizing current injections.

2.6. Immunohistochemical analysis

Immunohistochemistry or immunofluorescence experiments were performed with the following antibodies: anti-neuronal nuclei (NeuN, Chemicon, Temecula, CA, USA, 1:3000) to evaluate neuronal density and cell loss; anti-calbindin (CB, Swant, Bellinzona, Switzerland, 1:5000) to visualize calbindin expression and subfields of hippocampus; anti-doublecortin (DCX, Cell Signaling, Danvers, MA, USA, 1:800) as marker of newly generated cells in subgranular cell layer of the dentate gyrus, and anti-ionized calcium binding adapter molecule 1 (Iba-1, Abcam, Cambridge, UK, 1:1000) to evaluate microglial features. Quantitative field fraction analysis on NeuN and CB-stained sections was performed.

2.7. Statistical analysis

Experiments were performed blind to genotype. Statistical analyses were performed with Prism V6.01 (GraphPad, La Jolla, USA). The normality of the data distribution was verified with the Shapiro-Wilk's test. Differences between groups were measured when appropriate using the two-tailed *t*-test, one-way analysis of variance (ANOVA), two-way ANOVA (*e.g.* Genotype × Treatment) or repeated measures two-way ANOVA. The ANOVA was followed by Tukey's or Sidak's *post hoc* tests. Survival curves were compared with the Log-rank (Mantel-Cox) test and the analysis of the data concerning the SIH or SIF protocols was performed with the Kruskal-Wallis test. When normality was not observed, the Mann Whitney test was used. Error bars represent standard error to the mean (SEM). Null hypotheses were rejected at the 0.05 level. Statistical significances are represented by the following *P*-values in all Figures: $*p < .05$; $**p < .01$; $***p < .001$; $****p < .0001$ and N = number of animals or n = number of cells for patch clamp recordings.

3. Results

3.1. SIH induces a severe long lasting epileptic phenotype in *Scn1a*$^{RH/+}$ mutant mice

We optimized a protocol for induction of repeated short seizures by hyperthermia (SIH) in *Scn1a*$^{RH/+}$ mice in the period of seizure onset for *Scn1a* mouse models (Fig. 1A; see material and methods).

We evaluated different parameters during the SIH protocol, namely: survival, seizure occurrence, temperature threshold for seizure occurrence and seizure severity. *Scn1a*$^{RH/+}$-SIH mice was the only group showing behavioral seizures during the SIH protocol and presented the lowest survival (Fig. 1B–C). Moreover, the temperature threshold required for seizure induction increased in the first 3 days, consistent with an adaptive compensation in response to the SIH protocol, which did not persist, as from day 3 it returned to the initial values (Suppl. Fig. 1A). The severity of seizures increased from clonic at day 1 to generalized tonic-clonic seizures at day 4 (Fig. 1C; see Supplementary material for seizure severity scale).

To determine if the SIH protocol could induce long-lasting spontaneous seizures, we performed synchronized video-ECoG recordings after the end of the SIH protocol for a period of 7 weeks. Though, previous studies reported that *Scn1a*$^{RH/+}$ mice in the C57BL/6J background show sporadic spontaneous seizures (Dutton et al., 2017; Martin et al., 2010), we could not observe spontaneous GTC seizures in *Scn1a*$^{RH/+}$ mice in the 129:B6 background (Fig. 1E, Suppl. Table 1). In *Scn1a*$^{RH/+}$ mice, however, the SIH protocol induced the appearance of a long-lasting epileptic phenotype, with relatively frequent spontaneous GTC seizures that did not remit during the seven-week period of video-ECoG recordings (Fig. 1D–E, Suppl. Table 1). We also observed interictal spikes (Fig. 1F), which we quantified at P60 observing that they were present in almost all the *Scn1a*$^{RH/+}$-SIH mice, but never in *Scn1a*$^{RH/+}$ control mice (Fig. 1G). These results shows that apparently asymptomatic *Scn1a*$^{RH/+}$ mice are vulnerable to develop chronic epilepsy upon the SIH protocol.

3.2. SIH induces long-lasting dysfunctions in behavioral/cognitive phenotypes in *Scn1a*$^{RH/+}$ mice

To find out if *Scn1a*$^{RH/+}$-SIH mice exhibit long lasting features of EE, in particular DS-like, we performed cognitive and behavioral tests in adult mice at P60–90. We first used the open field (OF) test to evaluate locomotor/exploratory activity (average speed, distance travelled and rearing episodes). *Scn1a*$^{RH/+}$-SIH mice travelled a greater total distance at a higher average speed and presented an increase of the number of rearing events (Fig. 2A–D), whereas WT (control and SIH) and *Scn1a*$^{RH/+}$ mice had similar features (Fig. 2A–D). Thigmotaxis was however unchanged in *Scn1a*$^{RH/+}$–SIH mice, suggesting no alterations in anxiety (Fig. 2E), as confirmed also by the dark/light box test (Suppl. Fig. 2A). Stereotyped repetitive behaviors (number of body rotations during the OF) were increased only in *Scn1a*$^{RH/+}$-SIH mice (Fig. 2F). Circadian cycle of activity was evaluated in the four groups for 68 consecutive hours in an actimeter. All groups displayed a clear circadian cycle (Fig. 2G–H) (low activity during light/resting phase and higher activity during dark/active phase). Horizontal activity was similar in all groups (Fig. 2G). Vertical activity of *Scn1a*$^{RH/+}$-SIH mice was increased during the first 12 h (1st night) (Fig. 2H), confirming a novelty-induced hyperactivity.

Sociability skills were tested in the three-chamber test. *Scn1a*$^{RH/+}$-SIH had impaired sociability and social novelty skills (Fig. 2I–J). This group did not prefer the stranger mouse (M) compared to the empty cage during the sociability phase nor the new mouse (nM) compared to the familiar mouse (fM) during the social novelty phase, differently than the other groups. These results could not be explained by chamber preference, as confirmed in the habituation phase (Suppl. Fig. 2B). Yet, the *Scn1a*$^{RH/+}$-SIH mice travelled at higher speed during this habituation phase (Suppl. Fig. 2C), showing a novelty-associated hyperactivity that normalised during the sociability and social novelty phases (Suppl. Fig. 2D–E).

Hippocampus-dependent spatial learning and long-term memory in the Morris water maze (MWM) were impaired in *Scn1a*$^{RH/+}$-SIH mice (Fig. 3A). In the two days of cue task we evaluated the latency to reach the visible platform. Though the *Scn1a*$^{RH/+}$-SIH had a higher latency to reach the platform at D1, all groups behave similarly at D2 (Fig. 3A), arguing against sensory-motor deficits. In the spatial training all groups improved their performance from D1 to D4, but *Scn1a*$^{RH/+}$-SIH mice showed longer escape latencies (Fig. 3A) even if the initial performance during trial 1 of D1 was identical to other groups (Fig. 3B). The poorer

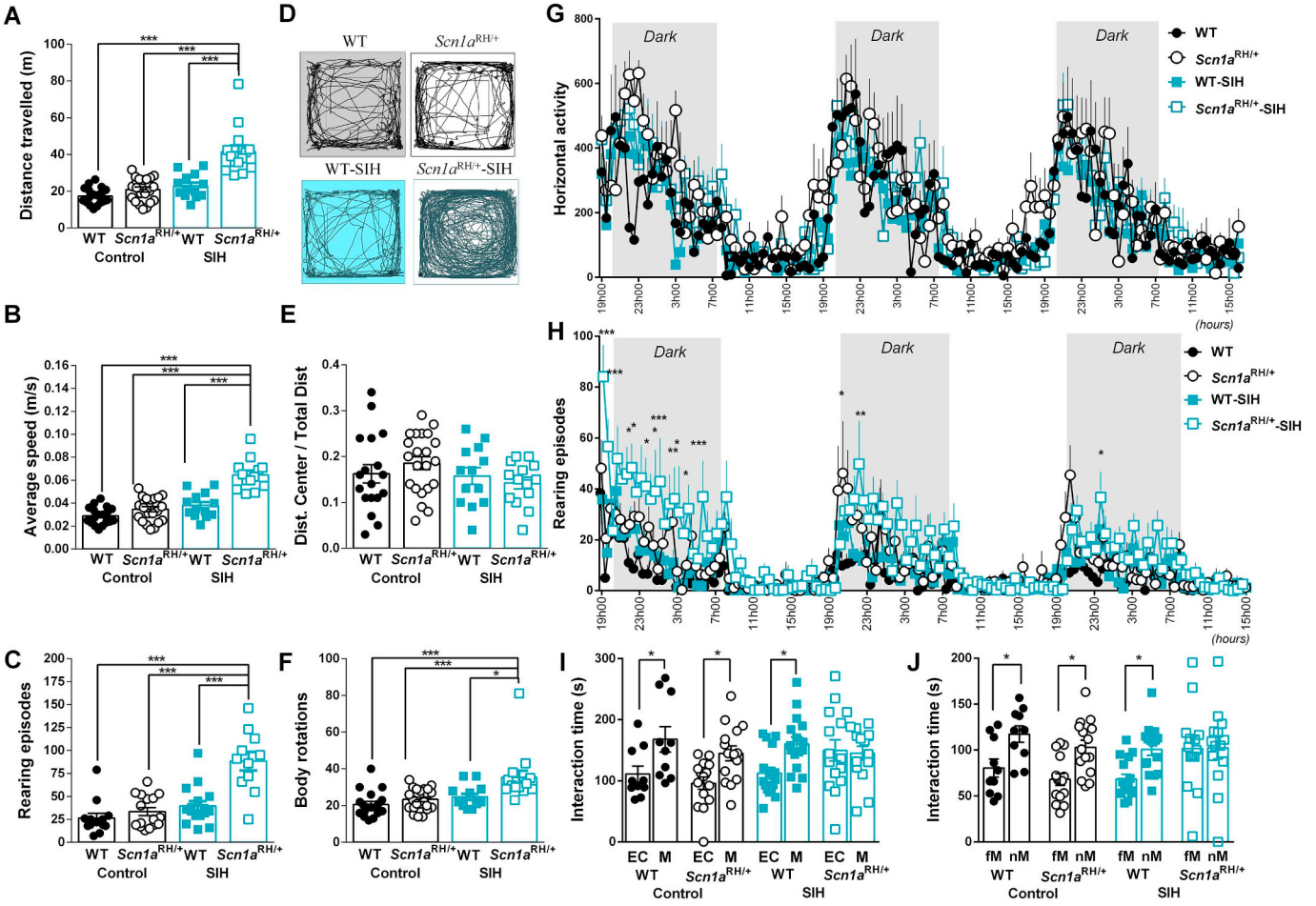

Fig. 2. *Scn1a*$^{RH/+}$-SIH mice display a novelty-associated increase in activity, stereotyped behavior and impaired sociability skills.
A–F: Analysis from the Open Field (10 min); A: Distance travelled and B: Average speed (WT $N = 19$, *Scn1a*$^{RH/+}$ $N = 22$, WT-SIH $N = 13$, *Scn1a*$^{RH/+}$-SIH $N = 14$). C: Number of rearing episodes (WT N = 13, *Scn1a*$^{RH/+}$ $N = 16$, WT-SIH $N = 11$, *Scn1a*$^{RH/+}$-SIH N = 11). D: Track plots of the locomotor activity. E: Thigmotaxis measured as the distance travelled in the center divided by the total distance travelled (WT N = 19, *Scn1a*$^{RH/+}$ N = 22, WT-SIH N = 13, *Scn1a*$^{RH/+}$-SIH N = 14). F: Full body rotations (WT N = 19, *Scn1a*$^{RH/+}$ N = 22, WT-SIH N = 13, *Scn1a*$^{RH/+}$-SIH N = 14). G–H: Actimeter analysis scored for 68 consecutive hours (data showed by 30 min periods) (WT $N = 5$, *Scn1a*$^{RH/+}$ $N = 9$, WT-SIH $N = 8$, *Scn1a*$^{RH/+}$-SIH N = 9); G: Total horizontal activity. H: Total vertical activity (number of rearing episodes). I–J: Sociability skills in the 3-chamber social interaction test (WT N = 10, *Scn1a*$^{RH/+}$ $N = 15$, WT-SIH N = 16, *Scn1a*$^{RH/+}$-SIH N = 14); I: Social interaction time (s), EC: Empty Cage; M: Mouse. J: Social novelty interaction time (s), fM: familiar Mouse; nM: new Mouse. See Supplementary Statistics Tables for details on statistics.

performance was not justified by a decrease in swim speed, which was instead higher and with a longer distance travelled (Suppl. Fig. 2F–G).

Long-term memory was tested with a probe trial 24 h after training completion. *Scn1a*$^{RH/+}$-SIH mice spent less time in the target quadrant than the other groups and did not discriminate between target quadrant and adjacent quadrants (Fig. 3C), as clearly shown by the trajectories in Fig. 3D. Also, the number of crosses in the platform zone was significantly decreased for *Scn1a*$^{RH/+}$-SIH mice (Fig. 3E). Thus, *Scn1a*$^{RH/+}$-SIH mice are less precise in remembering the previous platform placement.

We assessed working memory in a radial maze, following the protocol illustrated in Fig. 3F. The *Scn1a*$^{RH/+}$-SIH mice did not reach the criterion of > 75% correct choices for two consecutive days as observed for the other 3 groups at D9 and D10, consistent with a significantly lower performance in the task (Fig. 3G).

Thus, WT, WT-SIH and *Scn1a*$^{RH/+}$ mice performed equally well in these behavioral and cognitive tasks, while *Scn1a*$^{RH/+}$-SIH mice exhibited clear novelty-associated hyperactivity, exacerbated stereotyped behavior, sociability, spatial learning and working memory impairments. These data indicate that the R1648H mutation *per se* does not promote behavioral or cognitive phenotypes in this genetic background, but that seizures at the age of the disease onset in these models precipitate this mild/asymptomatic phenotype into a severe phenotype lasting till adulthood.

3.3. SIH does not cause major cytoarchitectural modifications in the hippocampus of *Scn1a*$^{RH/+}$ mice

We investigated the presence of hippocampal and cellular alterations in *Scn1a*$^{RH/+}$ mice at P60. In fact, we previously showed that the hippocampus is implicated in the generation of hyperthermic seizures in a knock-out *Scn1a* model of DS (Liautard et al., 2013) and hippocampal dysfunction has been reported in several *Scn1a* mutant mouse lines (Han et al., 2012; Kaplan et al., 2017; Mistry et al., 2014; Tsai et al., 2015; Yu et al., 2006). We observed that Nissl (Fig. 4A–B) and NeuN (Fig. 4C–D & G) staining did not reveal major cytoarchitectural modifications or cell loss in *Scn1a*$^{RH/+}$-SIH mice. Doublecortin (DCX) staining of the newly generated cells in the subgranular zone of the dentate gyrus (DG) was also similar in *Scn1a*$^{RH/+}$-SIH and *Scn1a*$^{RH/+}$ mice suggesting normal neurogenesis (Suppl. Fig. 3A–B). Moreover, immunolabeling for ionized calcium binding adapter molecule 1 (Iba-1), a marker of activated microglia, showed no microglia activation (thus absence of this sign of inflammation) in *Scn1a*$^{RH/+}$-SIH mice (Suppl. Fig. 3C–D). Although the expression of calbindin (CB) in

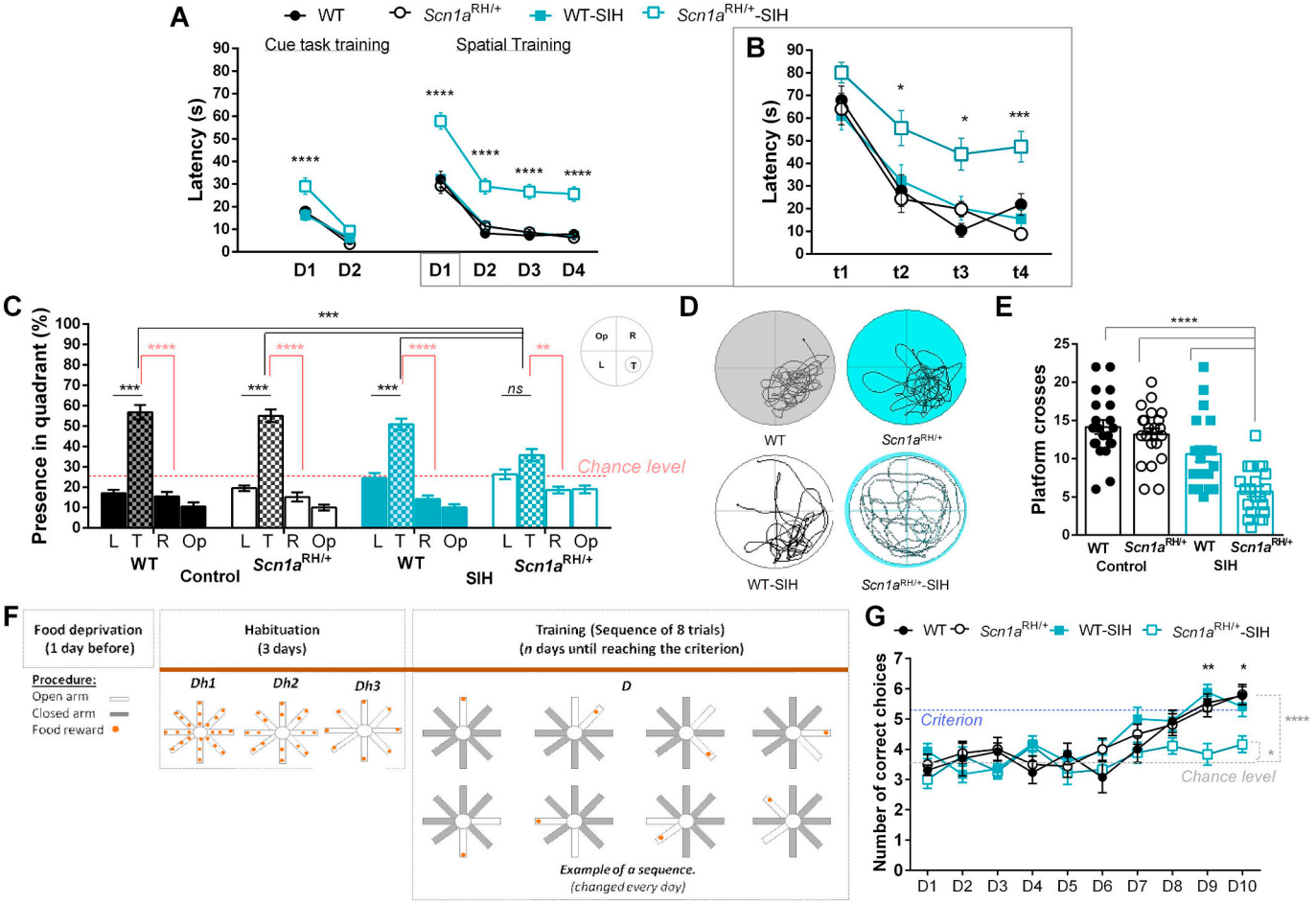

Fig. 3. *Scn1a*$^{RH/+}$-SIH mice exhibit impaired spatial and working memories.
Mice were tested (A–E) for spatial learning with the Morris Water Maze task (WT N = 19, *Scn1a*$^{RH/+}$ N = 22, WT-SIH *N* = 23, *Scn1a*$^{RH/+}$-SIH *N* = 21) and (F–G) for working memory in the 8-arms radial maze (WT N = 13, *Scn1a*$^{RH/+}$ N = 16, WT-SIH *N* = 17, *Scn1a*$^{RH/+}$-SIH *N* = 18). A: Data presented for cue task and spatial training represent average latencies to find the platform of four trials per day (D). B: Plot of the latency to find the platform in the four trials of D1 spatial training. C: Probe test: 24 h after training completion, the platform was removed and the proportion of time spent searching the platform in each of the four quadrants of the pool during 60 s of swimming is reported (L: Left, T: Target, R: Right, Op: Opposite). The persistence in the target quadrant is compared to chance level (considered at 25%) (dotted line). D: Representative track plots during probe test. E: Measures of the number of crosses in the enlarged "platform zone". F: Protocol timeline for the radial maze training: each training day had 8 trials, with the sequence of open arms changed every day (an example of a sequence is illustrated). G: Number of correct choices per day during the working memory training. Two dotted lines represent: the criterion corresponding to 75% of 7 correct choices (5.25), and the chance level corresponding to 50% of 7 choices (3.5). See Supplementary Statistics Tables for details on statistics.

Ammon's Horn was comparable in *Scn1a*$^{RH/+}$-SIH and *Scn1a*$^{RH/+}$ mice, CB signal in the DG of *Scn1a*$^{RH/+}$-SIH was significantly reduced (Fig. 4E–F & H). Therefore, SIH does not induce major neurohistological modifications in *Scn1a*$^{RH/+}$ mice, but a reduction of CB signal in the DG.

3.4. *Scn1a*$^{RH/+}$ SIH mice show an increase in firing frequency of DG granule neurons but not of CA1 pyramidal neurons

We performed whole-cell current-clamp recordings to assess the excitability of DG granule cells and CA1 pyramidal neurons, because of our data on altered CB expression in the DG and of previous studies that have reported altered excitability of excitatory neurons as a possible pathologic remodeling in *Scn1a* mouse models (Favero et al., 2018; Mistry et al., 2014). We compared input-output relationships and found that excitability of *Scn1a*$^{RH/+}$-SIH CA1 neurons was not significantly modified (Fig. 4I–J). By contrast, DG granule neurons of *Scn1a*$^{RH/+}$-SIH mice were strongly hyperexcitable compared to other groups (Fig. 4K–L). Importantly, neither the mutation itself (WT *vs* *Scn1a*$^{RH/+}$) nor the SIH protocol itself (WT *vs* WT-SIH) affected *per se* the intrinsic excitability properties of the two populations of neurons. Passive membrane properties and resting potential did not significantly differ between genotypes/treatments in both CA1 and DG (data not shown). This data demonstrates that, while the R1648H *per se* does not significantly modify the excitability of CA1 or DG excitatory neurons, seizures can induce long-term modifications of DG granule cell excitability, and the mutation is necessary for this neuronal subtype-specific pathological remodeling.

3.5. Induction of short seizures in WT and Scn1a$^{RH/+}$ mice using flurothyl

Febrile and hyperthermic seizures are characteristic in *SCN1A* epilepsies. However, with the SIH protocol, we could not determine if the R1648H mutation is necessary for generating the observed seizure-induced phenotypes or if seizures could be sufficient. Thus, we tested if chemically induced short-lasting seizures could be sufficient *per se* to induce these long-term alterations. We induced seizures in both WT and *Scn1a*$^{RH/+}$ mice using the convulsant flurothyl (Martin et al., 2007, 2010), with a protocol (SIF) harboring the same features as the SIH protocol (number and duration of seizures) (Fig. 5A). Same parameters considered during SIH were measured for SIF. The mortality rate of *Scn1a*$^{RH/+}$-SIF (comparable to that induced by the SIH protocol, in grey

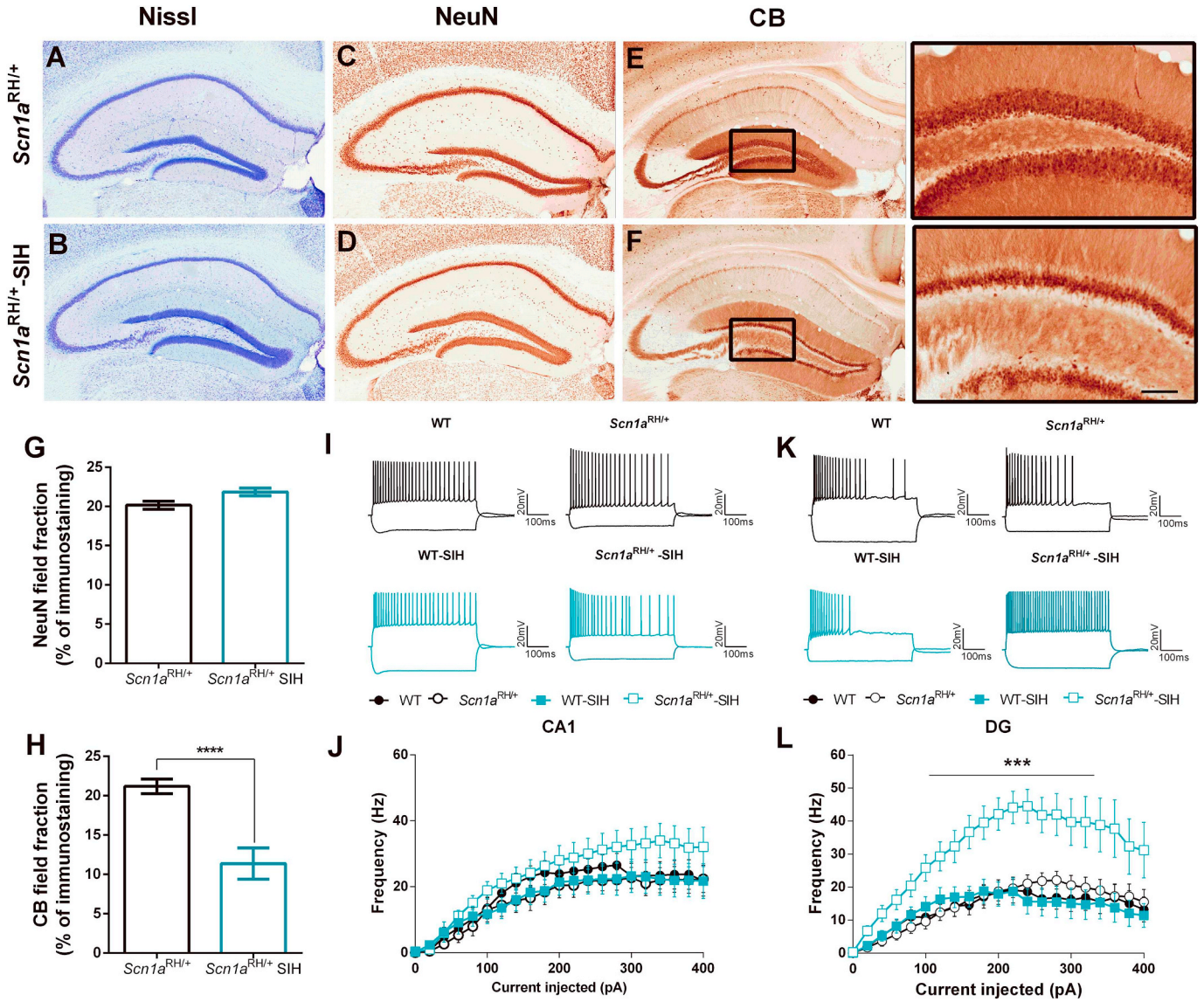

Fig. 4. No major cytoarchitectural modifications, but reduced calbindin staining and increased DG granule cell excitability in the hippocampus of *Scn1a*$^{RH/+}$-SIH mice.

A–F: Representative immunostaining images for the hippocampus of *Scn1a*$^{RH/+}$ and *Scn1a*$^{RH/+}$-SIH mice at P60 (scale bar; A-F: 500 μm, enlarged area: 100 μm); A–B: Nissl-Cresyl violet staining, C-D: NeuN immunostaining, and E–F: calbindin (CB) immunostaining (with enlarged areas shown in E–F to the right). G–H: Quantification of immunostainining signal for NeuN (G) and CB (H) in DG ($N = 6$). I,K: Representative membrane potential traces recorded with injections of 200pA depolarizing or hyperpolarizing currents in CA1 pyramidal neurons and DG granule cells (respectively) from brain slices for the four groups. J,L: Input-output relationship of the firing frequency measured as the number of action potentials per second (Hz) when neurons were depolarized by current steps of increasing amplitude (20pA steps with 550 ms duration), for CA1 pyramidal neurons (WT $n = 10$, *Scn1a*$^{RH/+}$ $n = 13$, WT-SIH $n = 11$, *Scn1a*$^{RH/+}$-SIH n = 11) and DG granule cells (WT n = 13, *Scn1a*$^{RH/+}$ $n = 12$, WT-SIH n = 12, *Scn1a*$^{RH/+}$-SIH n = 10) as indicated. See Supplementary Statistics Tables for details on statistics.

in Fig. 5B) was larger than for WT-SIF mice (Fig. 5B), although the severity of seizures induced by SIF in both groups was similar (Fig. 5C) and comparable to that of *Scn1a*$^{RH/+}$-SIH mice during the SIH protocol (in grey in Fig. 5C).

3.6. SIF also induces a severe epileptic phenotype and neuronal remodeling in *Scn1a*$^{RH/+}$ but not in WT mice

We performed long lasting video-ECoG recordings after the induction of seizures. We observed that *Scn1a*$^{RH/+}$-SIF mice exhibited spontaneous GTC seizures for several weeks after SIF (Fig. 5D–E) (as seen with SIH, grey trace) and interictal spikes, which we quantified at P60 (Fig. 5F–G). None of these epileptic phenotypes were observed in WT-SIF mice (Fig. 5D–E & Suppl. Table 1). Moreover, DG granule neurons were hyperexcitable only in *Scn1a*$^{RH/+}$-SIF mice (Fig. 5H–I), as in *Scn1a*$^{RH/+}$-SIH.

3.7. SIF induces long-lasting behavioral/cognitive dysfunctions in *Scn1a*$^{RH/+}$ but not in WT mice

We also evaluated the long-term cognitive and behavioral consequences of the SIF protocol (Fig. 5A). In the open field, we observed that SIF induced an increase in distance travelled, average speed, rearing episodes and stereotyped behavior only in *Scn1a*$^{RH/+}$-SIF mice (Fig. 6A–E). Thigmotaxis was similar in the two groups (Suppl. Fig. 4A). When tested for sociability skills, *Scn1a*$^{RH/+}$-SIF mice did not exhibit sociability (Fig. 6F) or social novelty (Fig. 6G) preference contrasting to the WT-SIF group. The lack of sociability skills in *Scn1a*$^{RH/+}$-SIF was not caused by chamber preferences (Suppl. Fig. 4B) or by locomotor differences (Suppl. Fig. 4D–E). The increase in activity was observed

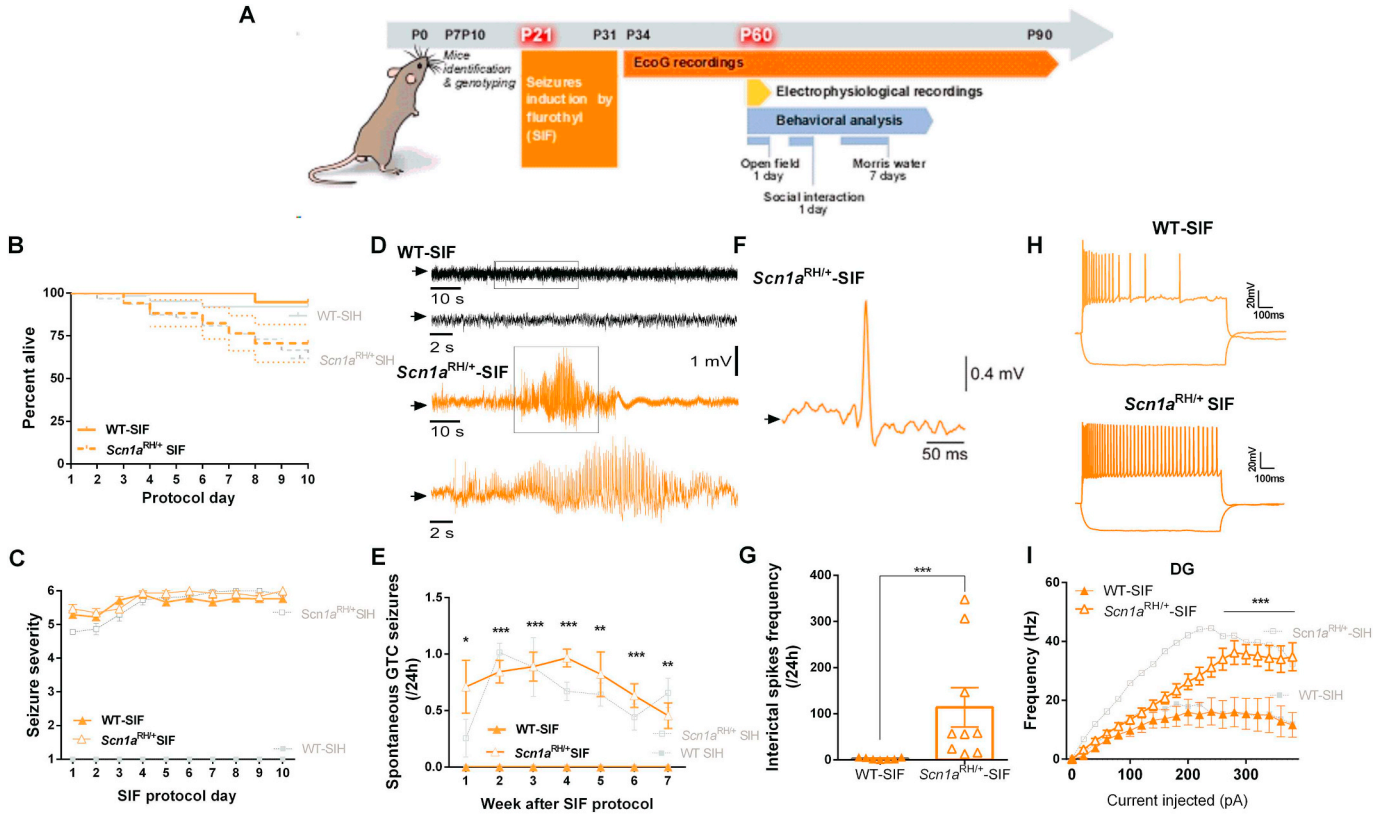

Fig. 5. The SIF protocol worsens the epileptic phenotype only in *Scn1a*$^{RH/+}$ mutant mice.
A: Protocol timeline sequence of experiments from P7 to P90. All groups went through identification and genotyping, then they were submitted to the SIF protocol at P21-31, followed by either ECoG recordings, behavioral analysis or electrophysiological recordings. B: Percentage survival of WT-SIF and *Scn1a*$^{RH/+}$-SIF at end of SIF protocol (WT-SIF *N* = 19, *Scn1a*$^{RH/+}$-SIF N = 17). C: Seizure severity during SIF (WT-SIF N = 19, *Scn1a*$^{RH/+}$-SIF N = 17). D: Representative ECoG traces recorded ats P40, in WT-SIF or *Scn1a*$^{RH/+}$-SIF mice, as indicated, showing normal activity in a WT-SIF mouse and activity during a generalized tonic-clonic seizure in a *Scn1a*$^{RH/+}$-SIF mouse (including end of pre-ictal, ictal and initial post-ictal periods). The parts highlighted by the boxes, correponding to ictal period in the *Scn1a*$^{RH/+}$-SIF recording, are dysplayed below the trace at a higher time resolution. The black arrows indicate 0 mV. E: Average spontaneous GTC seizure frequency per 24 h observed for 7 weeks in WT-SIF (*N* = 7) and *Scn1a*$^{RH/+}$-SIF mice (*N* = 9) from P34 to P90. F: Representative interictal spike recorded at P60 in a *Scn1a*$^{RH/+}$-SIF mouse; the black arrow indicates 0 mV. G: Interictal spikes' frequency (events/24 h) recorded at P60 in WT-SIF (*N* = 7) and *Scn1a*$^{RH/+}$-SIF mice (N = 9). H: Representative membrane voltage traces at 300 pA current injection recorded from DG granule cells in WT-SIF and *Scn1a*$^{RH/+}$-SIF hippocampal slices. I: Input-output relationship of the firing frequency measured as the number of action potentials per second (Hz) when DG granule cells were depolarized by current steps of increasing amplitude (20pA steps with 550 ms duration) in WT-SIF (*n* = 9) and *Scn1a*$^{RH/+}$-SIF (n = 10) hippocampal slices. In panels B, C, E, and I, grey traces are data obtained with the SIH protocol from Figs. 1 and 4, displayed for comparison. See Supplementary Statistics Tables for details on statistics.

only in the habituation phase, suggesting a novelty-associated hyperactivity (Suppl. Fig. 4C).

In the MWM task, the *Scn1a*$^{RH/+}$-SIF mice showed a worst performance than the WT-SIF in the learning phases of the task (cue task, spatial learning test, Fig. 6H) with an increase in the distance travelled but global normal speed (Suppl. Fig. 4F–G). During the probe test both groups spent more time in the target quadrant, at higher level than chance, but only the WT-SIF mice discriminated between adjacent quadrants (Fig. 6I).

Altogether, our results indicate that the SIF protocol differently affected WT and mutant mice, causing long-term behavioral and cognitive deficits only in *Scn1a*$^{RH/+}$ mice. Indeed, the *Scn1a*$^{RH/+}$-SIF group exhibited novelty-induced hyperactivity, stereotyped behavior, deficits of sociability and spatial learning and memory, phenotypes identical to *Scn1a*$^{RH/+}$ mice submitted to the SIH protocol (light grey data in Fig. 6 for comparison).

3.8. Short repeated seizures induce modifications of brain rhythms in both Scn1a$^{RH/+}$ *and WT mice*

Seizures-associated global alterations of brain rhythms were assessed through spectral analysis of ECoG recordings. We performed a longitudinal analysis over the period P34-P90 in mutant mice after SIH or SIF protocols (*Scn1a*$^{RH/+}$-SIH and *Scn1a*$^{RH/+}$-SIF mice). Fig. 7A shows representative power spectral profiles of *Scn1a*$^{RH/+}$, *Scn1a*$^{RH/+}$-SIH and *Scn1a*$^{RH/+}$-SIF mice in a 7-day period; the global analysis is displayed in Fig. 7B–E and is based on the average of the whole period. The analysis focused on theta (4–12 Hz) and gamma (60–100 Hz) bands (Fig. 7A–E) of power spectra, which relate to specific functions of neuronal circuits. The induction of seizures by both protocols, SIH and SIF, did not modify the total spectral power (Fig. 7C) or the relative power of the gamma band (Fig. 7E) compared to control *Scn1a*$^{RH/+}$ mice, but increased the relative power of the theta frequency peak (Fig. 7D).

We performed a more detailed analysis discriminating the vigilance-states in a 24 h period at P60 (Fig. 7F–L), the age at which animals were submitted to behavioral tasks. Rapid eye movement (REM) sleep, slow wave sleep (SWS) and awake periods (AW) were distinguished. We compared the same spectral features considered for the longitudinal study, but selecting periods without ictal or interictal epileptiform activity, to focus the analysis on non-epileptic brain activity. Fig. 7F shows representative ECoG traces during REM sleep, and Fig. 7G–I the power spectra according to vigilance state. We observed that SIF had higher impact on brain rhythms, seen by the increase in total power in all vigilance states (Fig. 7J) and the increase in relative theta peak power in the AW period (Fig. 7K). The relative gamma power was lower

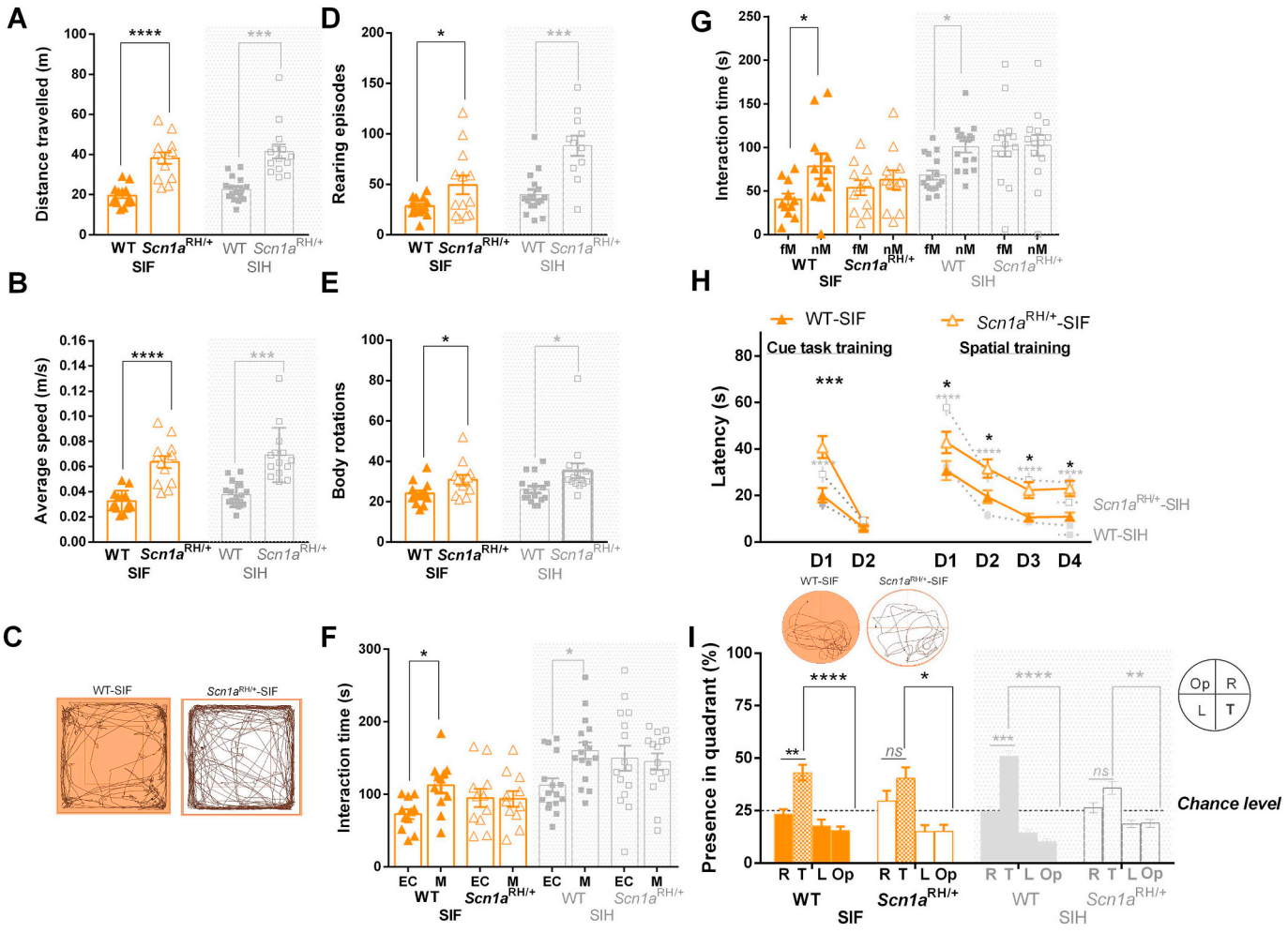

Fig. 6. Seizures induced with flurothyl cause behavioral and cognitive dysfunctions in *Scn1a*$^{RH/+}$ mice but not in WT mice.
A–B: Quantification of locomotor activity of mice placed in the OF for 10 min, expressed as A: distance travelled and B: average speed (WT-SIF $N = 14$, *Scn1a*$^{RH/+}$-SIF $N = 13$). C: Track plots of locomotor activity in OF. D–E: Analysis of stereotyped behavior as D: Number of rearing episodes (WT-SIF N = 14, *Scn1a*$^{RH/+}$-SIF N = 13) and E: Full body rotations (WT-SIF N = 14, *Scn1a*$^{RH/+}$-SIF N = 13). F–G: Sociability skills in the 3-chamber social interaction test as F: Social interaction time (s), EC: Empty Cage; M: Mouse, and G: Social novelty interaction time (s), fM: familiar Mouse; nM: new Mouse (WT-SIF $N = 11$, *Scn1a*$^{RH/+}$-SIF N = 11). H–I: Spatial learning and memory in the MWM task: H: Latency to reach platform during cue task and spatial training (average of 4 trials per day (D)). I: Probe test (24 h after training completion) represented as proportion of time spent searching platform in the four quadrants (R: Right, T: Target, L: Left, Op: Opposite). The target quadrant (where the platform was located) is highlighted with a different pattern. Persistence in target quadrant is compared to chance level (considered at 25%) (dotted line). In all panels, except C, grey traces represent data obtained with SIH protocol from Figs. 2 and 3, displayed for comparison. See Supplementary Statistics Tables for details on statistics.

for both *Scn1a*$^{RH/+}$-SIH and *Scn1a*$^{RH/+}$-SIF mice in AW periods than in the control *Scn1a*$^{RH/+}$ mice (Fig. 7L). Both vigilance-state analysis and longitudinal analysis at P60 showed that seizures increase the theta peak power. Moreover, vigilance-state analysis showed for some states increased total power and decreased gamma power.

To investigate the effect of seizures *per-se* on brain rhythms, we performed similar analyses of ECoG recordings obtained in WT-SIF, which underwent short repeated seizures, comparing to WT-SIH, which did not have seizures. Analysis of the longitudinal power spectra (Suppl. Fig. 5A–B) showed that the total power was not modified (Suppl. Fig. 5C), whereas relative theta power was increased (Suppl. Fig. 5D) and relative gamma power was decreased in WT-SIF (Suppl. Fig. 5E). The vigilance-state dependent analysis at P60 of periods without epileptic activity (Suppl. Fig. 5F–L) showed an increase in total power spectra during REM sleep in WT-SIF (Suppl. Fig. 5J). WT-SIF relative theta peak power was higher both in REM sleep and in AW periods (Suppl. Fig. 5K), and the relative gamma power was decreased in AW periods (Suppl. Fig. 5L). Thus, WT-SIF animals, which experienced seizures, show alterations in brain rhythms that are qualitatively similar to the *Scn1a*$^{RH/+}$-SIH and *Scn1a*$^{RH/+}$-SIF mice, notably a clear increase of theta power, a state-dependent increase of total power and a decrease of gamma power.

4. Discussion

4.1. Short repeated hyperthermic seizures transform the asymptomatic phenotype of *Scn1a*$^{RH/+}$ mice into a severe DS-like phenotype

Febrile seizures are the most common pediatric seizures, which are in general considered benign when their duration is < 15 min; more prolonged “complex” seizures or febrile *status epilepticus* are instead high risk factors for the development of epilepsy and co-morbidities (Patterson et al., 2013). These long febrile seizures are common in patients carrying DS *SCN1A* mutations (Ragona et al., 2011; Villeneuve et al., 2014; Wolff et al., 2006), but they are not predictors of phenotype severity (Cetica et al., 2017). Hyperthermia can induce seizures in WT rodent pups at around P10, and hyperthermic complex seizures or *status epilepticus* induced at this age can lead to spontaneous limbic seizures in a minority of animals, in which cognitive dysfunctions are not always observed (Dubé et al., 2007, 2009; McClelland et al., 2011; Notenboom

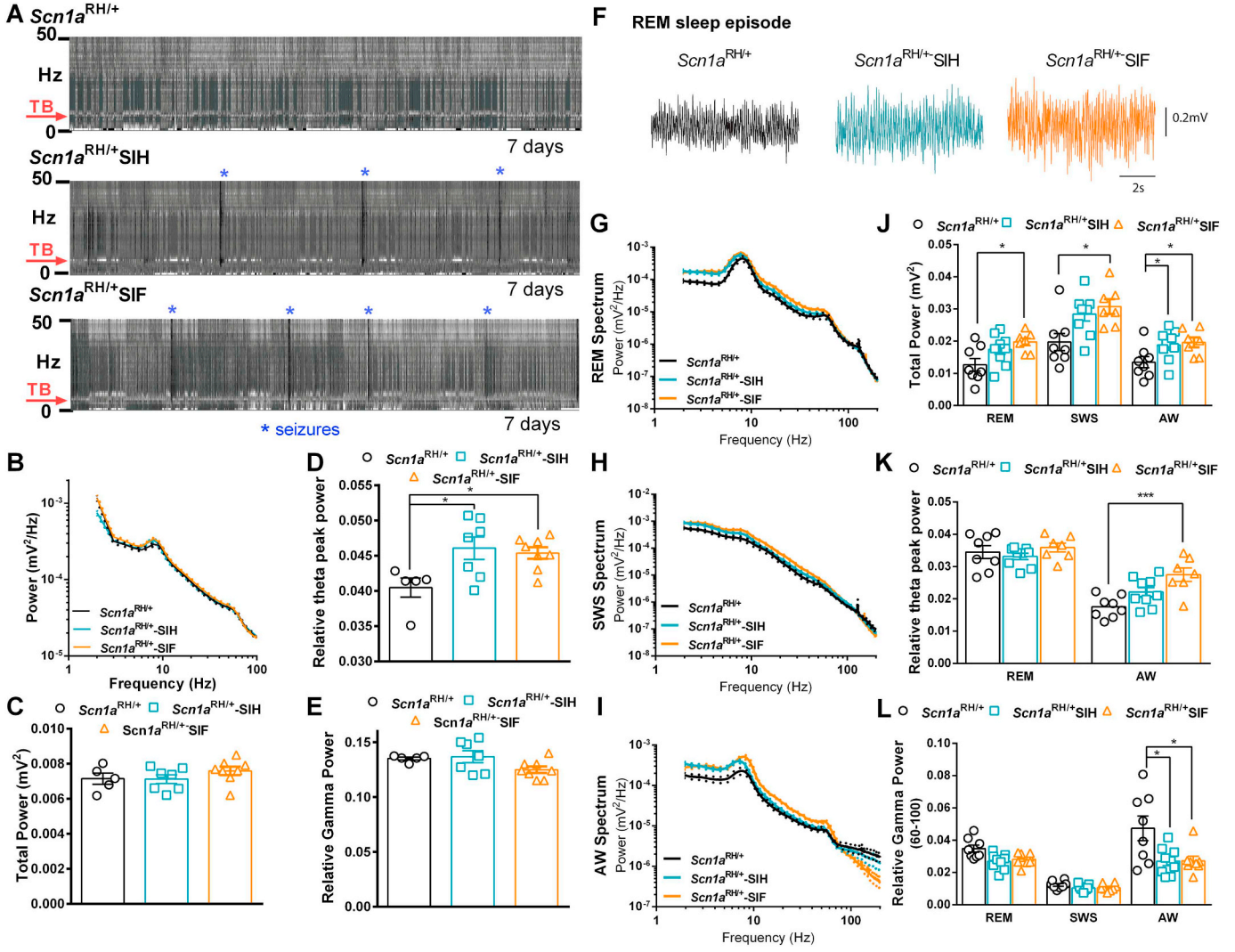

Fig. 7. Induced seizures cause ECoG spectral modifications in *Scn1a*$^{RH/+}$ mice.
A: Representative spectrograms of ECoG recordings, between 0 and 50 Hz, during 7 days selected from the whole 49-day recording period, the theta frequency band (TB) is indicated by the arrow. The cumulative power of different frequency bands is displayed in 1 min bins, with sequences of light/dark vertical columns indicating circadian 24 h ECoG power-density cycles. GTC seizures in *Scn1a*$^{RH/+}$-SIH and *Scn1a*$^{RH/+}$-SIF mice are highlighted with asterisks, and characterized by a long lasting post-ictal depression (generalized decrease in spectral power, visible as a dark vertical stripe in the diagram). B–E: Longitudinal analysis of the pooled average spectral powers for whole period of ECoG recordings for *Scn1a*$^{RH/+}$ ($N = 5$), *Scn1a*$^{RH/+}$-SIH ($N = 7$) and *Scn1a*$^{RH/+}$-SIF ($N = 8$) mice; B: Power spectrum pooled for the whole period of recording for each group. C: Total power quantified on the power spectrum; D: Peak power of the theta band (7–9 Hz) normalised to the total power. E: Power of the gamma band (60-100 Hz) normalised to the total power. F–L: Detailed spectral analysis performed on a 24 h window in periods without epileptiform activity at age P60 and differentiating REM sleep, slow wave sleep (SWS) and wake (AW) periods, from *Scn1a*$^{RH/+}$ (N = 8), *Scn1a*$^{RH/+}$-SIH (N = 8) and *Scn1a*$^{RH/+}$-SIF (N = 7) mice recordings; F: Representative ECoG traces recorded during REM sleep. G–I: power spectra of REM sleep (G), SWS (H) and AW (I) considering selected periods in the 24 h window. J: Total power quantified from the power spectra for the three vigilance states. K: Peak power of the theta band (7–9 Hz) normalised to the total power. L: Gamma (60-100 Hz) power normalised to the total power. See Supplementary Statistics Tables for details on statistics.

et al., 2010; Tao et al., 2016). Shorter recurrent hyperthermic seizures have been less studied, but some reports showed that they can induce memory dysfunctions and propensity to hyperexcitability of neuronal circuits, without an overt epileptic phenotype (Chang et al., 2003; Tsai and Leung, 2006). Recently, the effect of hyperthermic long seizures/*status epilepticus* has been investigated in *Scn1a*$^{RH/+}$ mice in the C57BL/6J genetic background, observing worsening of the epileptic phenotype and behavioral alterations (Dutton et al., 2017). However, as pointed out above, long seizures can induce these effects *per se*. We investigated the long-term effect of brief (< 1 min) and recurrent hyperthermic seizures (SIH protocol) induced in asymptomatic 129:B6 *Scn1a*$^{RH/+}$ mice at the age of seizure onset for *Scn1a* mouse models (Dutton et al., 2017; Oakley et al., 2009; Ogiwara et al., 2007), which correspond to the plateau for the expression of $Na_V1.1$ in mouse brain (Ogiwara et al., 2007). Notably, all *Scn1a*$^{RH/+}$ mice developed chronic spontaneous GTCs and interictal spikes after our SIH protocol, showing a much more severe epileptic phenotype than that observed after long seizures/*status epilepticus* (Dutton et al., 2017).

SIH also induced important behavioral and cognitive alterations in *Scn1a*$^{RH/+}$ mice, which were similar to the cognitive decline (deficits of language, attention, working and spatial memory) and behavioral dysfunctions (hyperactivity, repetitive behaviors and social interaction problems) exhibited by DS patients (Chieffo et al., 2011; Olivieri et al., 2016; Ragona et al., 2011; Villeneuve et al., 2014). Similar alterations (hyperactivity, social interaction deficits and impairments of learning and memory) were also reported in epileptic *Scn1a* DS mouse models (Han et al., 2012; Ito et al., 2013). A study performed with the *Scn1a*$^{RX/+}$ DS model also showed modifications of anxiety (Ito et al., 2013), which we did not observe in *Scn1a*$^{RH/+}$–SIH mice. Social interaction deficits were also reported in *Scn1a*$^{RH/+}$ mice after hyperthermic long

seizures/*status epilepticus* (Dutton et al., 2017). These deficits are considered autistic-like behaviors (Berkvens et al., 2015), although clinical studies have reported that autistic traits are mild, if present at all, in DS patients, and social interaction deficits could be instead due to their motor and cognitive deficits (Ceulemans, 2011; Villeneuve et al., 2014). *Scn1a*$^{RH/+}$ mice not submitted to the SIH protocol did not display behavioral/cognitive dysfunctions in our study. Mild dysfunctions in *Scn1a*$^{RH/+}$ mice have been observed in some studies (Purcell et al., 2013; Sawyer et al., 2016), but not in others (Dutton et al., 2017), and the difference could be mouse strain background-related.

Phenotype worsening in *Scn1a*$^{RH/+}$-SIH mice was not associated with overt neuronal loss, altered neurogenesis or microglia activation in the hippocampus. These effects are often observed in adulthood in rodent models of temporal lobe epilepsy, but not after induction of hyperthermic seizures/*status epilepticus* in rodent pups (Dubé et al., 2007; McClelland et al., 2011). Notably, in *Scn1a*$^{RH/+}$-SIH mice we observed a reduction of calbindin immunostaining in the DG, where it is expressed mainly by granule cells, and hyperexcitability of DG granule cells, consistent with a seizure-induced remodeling of their properties. Notably, CA1 pyramidal neurons' excitability remained unaltered. This is consistent with a neuronal-subtype specific pathological remodeling, with DG granule cells being particularly sensitive.

Overall, these results demonstrate that short recurrent hyperthermic seizures can cause remodeling of neuronal excitability in *Scn1a*$^{RH/+}$ mice and transform their phenotype from mild/asymptomatic to severe DS-like. Yet, they do not disclose if the genetic mutation is necessary for seizure-dependent phenotype worsening and remodeling.

4.2. The Scn1a mutation is necessary for seizure-dependent phenotype worsening and remodeling

To disclose the role of the mutation, we induced seizures in both *Scn1a*$^{RH/+}$ mice and WT littermates with the convulsant flurothyl (SIF) (Holmes et al., 1998), mimicking as close as possible seizure features observed with the SIH protocol. *Scn1a*$^{RH/+}$-SIF mice showed a DS-like phenotype that was identical to that of *Scn1a*$^{RH/+}$-SIH mice, as well as a similar remodeling of neuronal excitability. Importantly, flurothyl seizures did not induce phenotypic alterations and remodeling in WT littermates. Flurothyl has been used to evaluate the effects of seizures induced in WT rodent pups (up to 100 seizures induced between P1 and P15) (Holmes et al., 1998, 2015). This did not lead to spontaneous seizures, but induced memory and sociability deficits when tested 2–3 weeks after the induction. However, long term effects are more controversial because only very mild dysfunctions were observed after > 4 weeks (Barry et al., 2016; Huang et al., 1999). A recent study reported that induction of short seizures with flurothyl in adult C57BL/6J mice led to the appearance of spontaneous seizures, the frequency of which peaked in the first week after the end of the induction and remitted within one month (Kadiyala et al., 2016). Differences in the effect of Flurothyl-induced seizures in WT rodents could be age- or species/strain-related.

Altogether, our results demonstrate that the *Scn1a* genetic mutation/variant is necessary for the remodeling caused by short repeated seizures experienced in the period of disease onset for *Scn1a* mouse models, which lead to the induction of a severe persistent phenotype in apparently asymptomatic *Scn1a*$^{RH/+}$ mice, but have no significant effect in WT littermates. Notably, the effect is not dependent on the seizure trigger, because hyperthermia and flurothyl induced the same phenotype in mutant mice.

4.3. Dysfunctions of neuronal excitability in mouse models of Scn1a epileptogenic mutations

We have observed hyperexcitability of DG granule cells in adult *Scn1a*$^{RH/+}$ mice after induction of seizures, but not in pyramidal neurons from the CA1 area of the hippocampus. Hyperexcitability of pyramidal neurons in the CA3 area of the hippocampus has been observed in *Scn1a*$^{RH/+}$ mice after induction of hyperthermic long seizures/*status epilepticus* (Dutton et al., 2017), and increased excitability of pyramidal neurons of *Scn1a*$^{+/-}$ DS mice has been reported after the age of seizure onset (Mistry et al., 2014). However, the most consistent direct effect of epileptogenic *Scn1a* mutations is loss of function of $Na_V1.1$ channels, leading to hypoexcitability of GABAergic neurons (Favero et al., 2018; Guerrini et al., 2014; Hedrich et al., 2014; Ogiwara et al., 2007; Stern et al., 2017; Tsai et al., 2015; Yu et al., 2006). This effect is supported by the severe phenotype of conditional mouse models in which *Scn1a* was selectively deleted only in PV-positive GABAergic neurons (Dutton et al., 2013; Ogiwara et al., 2013; Rubinstein et al., 2015). Albeit at lower levels than in GABAergic neurons, $Na_V1.1$ is also expressed in excitatory neurons, in which DS mutations can cause mild hypoexcitability (De Stasi et al., 2016; Tai et al., 2014), ameliorating the phenotype of DS mouse models (Ogiwara et al., 2013). Thus, hyperexcitability of excitatory neurons is observed only in *Scn1a* mouse models that experienced seizures, consistent with an age- and neuron subtype-specific pathological remodeling induced by seizures. Notably, our results show that this remodeling is caused by the interaction between seizures and the *Scn1a* mutation.

4.4. Effect on brain rhythms

Alterations of EEG oscillations have been reported in DS patients (Holmes et al., 2012). Although brain rhythms are important for cognitive functions, these features had not thoroughly been investigated thus far in animal models of *Scn1a* mutations. Modifications of theta and delta rhythms have been reported in *Scn1a* knock-out mice (Kalume et al., 2015), and of gamma oscillations in mouse models of Alzheimer's disease (in which $Na_V1.1$ expression is reduced, leading to epileptiform activities) (Verret et al., 2012). We have quantified brain rhythms in ECoG recordings, focusing on theta and gamma rhythms because of their contribution to cognitive functions. The circadian pattern was conserved in all groups of mice, and the analysis showed that the main overall modifications were an increase of theta power and a decrease of gamma power in both *Scn1a*$^{+/-}$-SIH and *Scn1a*$^{+/-}$-SIF mice, although specific modifications were condition- and vigilance state-dependent. Notably, we observed similar effects in WT littermates after the SIF protocol. Therefore, these alterations could represent direct effects of seizures that do not depend on the *Scn1a* mutation, but they are not involved in the generation of the cognitive/behavioral dysfunctions that we observed, since WT-SIF mice display normal phenotype.

4.5. Potential clinical relevance of these findings

We examined two closely related questions with clinical relevance: the reasons for phenotypic variability of a given mutation in different individuals, and if seizures can induce severe phenotypes. Our results are not consistent with the concept of DS as pure channelopathy or DE (Scheffer et al., 2017), but suggest that seizures are important contributors to the development of severe phenotypes in carriers of *SCN1A* variants, and that therapeutic approaches should aim at reducing their occurrence as much as possible. This finding is important for DS/GEFS + mutations, but possibly also for more common epilepsies in which *SCN1A* variants have been identified as risk factors (Epi4K consortium and Epilepsy Phenome/Genome Project, 2017; EPICURE Consortium et al., 2012; ILAE, 2014; Kasperaviciute et al., 2013). *SCN1A* mutations/variants may increase the risk that seizures induce deleterious effects on the brain. In fact, in our model, the genetic mutation is important not only for inducing hyperexcitability in neuronal networks that triggers seizures, but also as a key element for the development of pathological remodeling and for long-lasting behavioral and cognitive dysfunctions induced by seizures, which are not directly linked to the effect of the mutation on the function of $Na_V1.1$ channels (Fig. 8). Notably, the pathological remodeling induced by the interaction

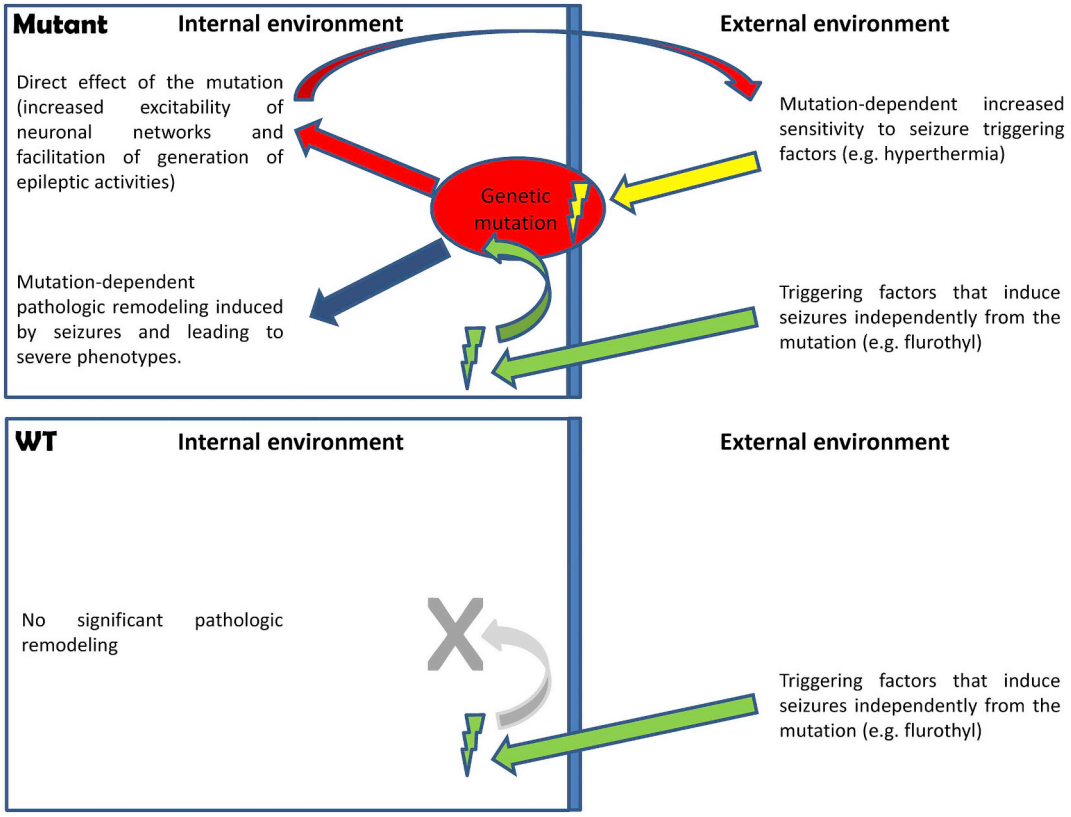

Fig. 8. Proposed model for the dual role of *Scn1a* mutations.
In our model the *Scn1a* mutation/variant (upper diagram) induces a direct effect increasing the excitability of neuronal networks (by decreasing excitability of GABAergic neurons): this is the initial mechanism that can reduce the threshold to seizure triggers. Additionally, short seizures generated through the direct initial effect of the mutation or by other factors (flurothyl in our experiments) at the age of disease onset for *Scn1a* mouse models can interact with the mutation for inducing pathologic remodeling (*e.g.* hyperexcitability of excitatory neurons), which leads to severe phenotypes. Notably, this remodeling is not directly linked to the initial effect of the mutation. Differently, similar seizures induced in wild type (WT) mice do not cause significant pathologic remodeling and do not lead to severe phenotypes (in our experiments we observed just mild modifications of brain rhythms).
Thus, we propose a dual role for the mutation/variant: facilitation of seizure triggering and interaction with seizures for inducing pathologic remodeling (above and beyond that induced by seizures alone or the mutation alone). This could be one of the mechanisms causing pleiotropy in patients carrying *SCN1A* mutations/variants and possibly other genetic mutations.

between mutation and seizures overcomes the effect of modifier genes that can improve the phenotype of *Scn1a* models and that have been recently identified comparing 129 and C57BL/6 mice (Hawkins et al., 2016). Mechanisms and factors that link mutations/variants and seizures to remodeling leading to pleiotropy should be better elucidated and could provide innovative therapeutic targets. Overall, our results are important for *SCN1A*-related disorders, but also as a general example for the identification of risk factors in a precision medicine framework.

Acknowledgements

We thank Nico Moshé for insightful suggestions, Sandrine Cestèle for discussions and help in setting up the SIH protocol, Franck Aguila for help with the graphic design of figures, and all the members of our laboratories for support.

Funding

This work was supported by the EC FP7 project DESIRE (Strategies for Innovative Research to improve diagnosis, prevention and treatment in children with difficult to treat Epilepsy) grant agreement n.: 602531 (to MM and HM) and the Investissements d'Avenir-Laboratory of Excellence “Ion Channel Science and Therapeutics” (grant LabEx ICST ANR-11-LABX-0015-01 to MM).

Authors' contribution

ARSP, IB, ME and MIS performed behavioral tests and analysis; FD and IB performed ECoG recordings and analysis; PP and AL performed patch-clamp recordings and analysis; CR and CF performed immunohistochemistry experiments and analysis; ARSP, MA and ME performed genotyping: VD, RG, VG and MM performed brain rhythm analysis; AE provided tools; HM, IB and MM conceived and coordinated the project; ARSP, FD, HM, IB and MM wrote the manuscript.

Appendix A. Supplementary data

Supplementary data to this article can be found online at https://doi.org/10.1016/j.nbd.2019.01.006.

References

Avanzini, G., Mantegazza, M., Terragni, B., Canafoglia, L., Scalmani, P., Franceschetti, S., 2018. The impact of genetic and experimental studies on classification and therapy of the epilepsies. Neurosci. Lett. 667, 17–26.
Balestrini, S., Sisodiya, S.M., 2018. Pharmacogenomics in epilepsy. Neurosci. Lett. 667, 27–39.
Baram, T.Z., Gerth, A., Schultz, L., 1997. Febrile seizures: an appropriate-aged model suitable for long-term studies. Brain Res. Dev. Brain Res. 98, 265–270.
Barry, J.M., Tian, C., Spinella, A., Page, M., Holmes, G.L., 2016. Spatial cognition following early-life seizures in rats: performance deficits are dependent on task demands. Epilepsy Behav. EB 60, 1–6.

Bender, A.C., Natola, H., Ndong, C., Holmes, G.L., Scott, R.C., Lenck-Santini, P.P., 2013. Focal Scn1a knockdown induces cognitive impairment without seizures. Neurobiol. Dis. 54, 297–307.
Berkovic, S.F., Mulley, J.C., Scheffer, I.E., Petrou, S., 2006. Human epilepsies: interaction of genetic and acquired factors. Trends Neurosci. 29, 391–397.
Berkvens, J.J., Veugen, I., Veendrick-Meekes, M.J., Snoeijen-Schouwenaars, F.M., Schelhaas, H.J., Willemsen, M.H., Tan, I.Y., Aldenkamp, A.P., 2015. Autism and behavior in adult patients with Dravet syndrome (DS). Epilepsy Behav. 47, 11–16.
Brunklaus, A., Ellis, R., Reavey, E., Semsarian, C., Zuberi, S.M., 2014. Genotype phenotype associations across the voltage-gated sodium channel family. J. Med. Genet. 51, 650–658.
Cetica, V., Chiari, S., Mei, D., Parrini, E., Grisotto, L., Marini, C., Pucatti, D., Ferrari, A., Sicca, F., Specchio, N., et al., 2017. Clinical and genetic factors predicting Dravet syndrome in infants with SCN1A mutations. Neurology 88, 1037–1044.
Ceulemans, B., 2011. Overall management of patients with Dravet syndrome. Dev. Med. Child Neurol. 53 (Suppl. 2), 19–23.
Chang, Y.-C., Huang, A.-M., Kuo, Y.-M., Wang, S.-T., Chang, Y.-Y., Huang, C.-C., 2003. Febrile seizures impair memory and cAMP response-element binding protein activation. Ann. Neurol. 54, 706–718.
Chieffo, D., Battaglia, D., Lettori, D., Del Re, M., Brogna, C., Dravet, C., Mercuri, E., Guzzetta, F., 2011. Neuropsychological development in children with Dravet syndrome. Epilepsy Res. 95, 86–93.
De Stasi, A.M., Farisello, P., Marcon, I., Cavallari, S., Forli, A., Vecchia, D., Losi, G., Mantegazza, M., Panzeri, S., Carmignoto, G., et al., 2016. Unaltered network activity and interneuronal firing during spontaneous cortical dynamics in vivo in a mouse model of severe myoclonic epilepsy of infancy. Cereb. Cortex N. Y. N 1991 (26), 1778–1794.
Depienne, C., Trouillard, O., Gourfinkel-An, I., Saint-Martin, C., Bouteiller, D., Graber, D., Barthez-Carpentier, M.A., Gautier, A., Villeneuve, N., Dravet, C., et al., 2010. Mechanisms for variable expressivity of inherited SCN1A mutations causing Dravet syndrome. J. Med. Genet. 47, 404–410.
Dravet, C., 2011. The core Dravet syndrome phenotype. Epilepsia 52 Suppl 2, 3–9.
Dubé, C.M., Brewster, A.L., Richichi, C., Zha, Q., Baram, T.Z., 2007. Fever, febrile seizures and epilepsy. Trends Neurosci. 30, 490–496.
Dubé, C.M., Zhou, J.-L., Hamamura, M., Zhao, Q., Ring, A., Abrahams, J., McIntyre, K., Nalcioglu, O., Shatskih, T., Baram, T.Z., et al., 2009. Cognitive dysfunction after experimental febrile seizures. Exp. Neurol. 215, 167–177.
Dutton, S.B., Makinson, C.D., Papale, L.A., Shankar, A., Balakrishnan, B., Nakazawa, K., Escayg, A., 2013. Preferential inactivation of Scn1a in parvalbumin interneurons increases seizure susceptibility. Neurobiol. Dis. 49, 211–220.
Dutton, S.B.B., Dutt, K., Papale, L.A., Helmers, S., Goldin, A.L., Escayg, A., 2017. Early-life febrile seizures worsen adult phenotypes in Scn1a mutants. Exp. Neurol. 293, 159–171.
Epi4K consortium, and Epilepsy Phenome/Genome Project, 2017. Ultra-rare genetic variation in common epilepsies: a case-control sequencing study. Lancet Neurol. 16, 135–143.
EPICURE Consortium, EMINet Consortium, Steffens, M., Leu, C., Ruppert, A.-K., Zara, F., Striano, P., Robbiano, A., Capovilla, G., Tinuper, P., et al., 2012. Genome-wide association analysis of genetic generalized epilepsies implicates susceptibility loci at 1q43, 2p16.1, 2q22.3 and 17q21.32. Hum. Mol. Genet. 21, 5359–5372.
Escayg, A., MacDonald, B.T., Meisler, M.H., Baulac, S., Huberfeld, G., An-Gourfinkel, I., Brice, A., LeGuern, E., Moulard, B., Chaigne, D., et al., 2000. Mutations of SCN1A, encoding a neuronal sodium channel, in two families with GEFS+2. Nat. Genet. 24, 343–345.
Favero, M., Sotuyo, N.P., Lopez, E., Kearney, J.A., Goldberg, E.M., 2018. A transient developmental window of fast-spiking interneuron dysfunction in a mouse model of Dravet syndrome. J. Neurosci. 38, 7912–7927.
Gataullina, S., Dulac, O., 2017. From genotype to phenotype in Dravet disease. Seizure 44, 58–64.
Guerrini, R., Marini, C., Mantegazza, M., 2014. Genetic epilepsy syndromes without structural brain abnormalities: clinical features and experimental models. Neurother. J. Am. Soc. Exp. Neurother. 11, 269–285.
Han, S., Tai, C., Westenbroek, R.E., Frank, H.Y., Cheah, C.S., Potter, G.B., Rubenstein, J.L., Scheuer, T., Horacio, O., Catterall, W.A., 2012. Autistic-like behaviour in Scn1a +/− mice and rescue by enhanced GABA-mediated neurotransmission. Nature 489, 385–390.
Hawkins, N.A., Zachwieja, N.J., Miller, A.R., Anderson, L.L., Kearney, J.A., 2016. Fine mapping of a Dravet syndrome modifier locus on mouse chromosome 5 and candidate gene analysis by RNA-seq. PLoS Genet. 12, e1006398.
Hedrich, U.B.S., Liautard, C., Kirschenbaum, D., Pofahl, M., Lavigne, J., Liu, Y., Theiss, S., Slotta, J., Escayg, A., Dihné, M., et al., 2014. Impaired action potential initiation in GABAergic interneurons causes hyperexcitable networks in an epileptic mouse model carrying a human Na(V)1.1 mutation. J. Neurosci. 34, 14874–14889.
Holmes, G.L., Gairsa, J.L., Chevassus-Au-Louis, N., Ben-Ari, Y., 1998. Consequences of neonatal seizures in the rat: morphological and behavioral effects. Ann. Neurol. 44, 845–857.
Holmes, G.L., Bender, A.C., Wu, E.X., Scott, R.C., Lenck-Santini, P.P., Morse, R.P., 2012. Maturation of EEG oscillations in children with sodium channel mutations. Brain Dev. 34, 469–477.
Holmes, G.L., Tian, C., Hernan, A.E., Flynn, S., Camp, D., Barry, J., 2015. Alterations in sociability and functional brain connectivity caused by early-life seizures are prevented by bumetanide. Neurobiol. Dis. 77, 204–219.
Huang, L., Cilio, M.R., Silveira, D.C., McCabe, B.K., Sogawa, Y., Stafstrom, C.E., Holmes, G.L., 1999. Long-term effects of neonatal seizures: a behavioral, electrophysiological, and histological study. Brain Res. Dev. Brain Res. 118, 99–107.
International League Against Epilepsy Consortium on Complex Epilepsies. Electronic address: epilepsy-austin@unimelb.edu.au, 2014. Genetic determinants of common epilepsies: a meta-analysis of genome-wide association studies. Lancet Neurol. 13, 893–903.
Ito, S., Ogiwara, I., Yamada, K., Miyamoto, H., Hensch, T.K., Osawa, M., Yamakawa, K., 2013. Mouse with Nav1.1 haploinsufficiency, a model for Dravet syndrome, exhibits lowered sociability and learning impairment. Neurobiol. Dis. 49, 29–40.
Kadiyala, S.B., Yannix, J.Q., Nalwalk, J.W., Papandrea, D., Beyer, B.S., Herron, B.J., Ferland, R.J., 2016. Eight flurothyl-induced generalized seizures lead to the rapid evolution of spontaneous seizures in mice: a model of epileptogenesis with seizure remission. J. Neurosci. 36, 7485–7496.
Kalume, F., Oakley, J.C., Westenbroek, R.E., Gile, J., de la Iglesia, H.O., Scheuer, T., Catterall, W.A., 2015. Sleep impairment and reduced interneuron excitability in a mouse model of Dravet syndrome. Neurobiol. Dis. 77, 141–154.
Kaplan, J.S., Stella, N., Catterall, W.A., Westenbroek, R.E., 2017. Cannabidiol attenuates seizures and social deficits in a mouse model of Dravet syndrome. Proc. Natl. Acad. Sci. U. S. A. 114, 11229–11234.
Kasperaviciute, D., Catarino, C.B., Matarin, M., Leu, C., Novy, J., Tostevin, A., Leal, B., Hessel, E.V.S., Hallmann, K., Hildebrand, M.S., et al., 2013. Epilepsy, hippocampal sclerosis and febrile seizures linked by common genetic variation around SCN1A. Brain J. Neurol. 136, 3140–3150.
Liautard, C., Scalmani, P., Carriero, G., de Curtis, M., Franceschetti, S., Mantegazza, M., 2013. Hippocampal hyperexcitability and specific epileptiform activity in a mouse model of Dravet syndrome. Epilepsia 54, 1251–1261.
Martin, M.S., Tang, B., Papale, L.A., Yu, F.H., Catterall, W.A., Escayg, A., 2007. The voltage-gated sodium channel Scn8a is a genetic modifier of severe myoclonic epilepsy of infancy. Hum. Mol. Genet. 16, 2892–2899.
Martin, M.S., Dutt, K., Papale, L.A., Dubé, C.M., Dutton, S.B., de Haan, G., Shankar, A., Tufik, S., Meisler, M.H., Baram, T.Z., et al., 2010. Altered function of the SCN1A voltage-gated sodium channel leads to gamma-aminobutyric acid-ergic (GABAergic) interneuron abnormalities. J. Biol. Chem. 285, 9823–9834.
McClelland, S., Dubé, C.M., Yang, J., Baram, T.Z., 2011. Epileptogenesis after prolonged febrile seizures: mechanisms, biomarkers and therapeutic opportunities. Neurosci. Lett. 497, 155–162.
Mistry, A.M., Thompson, C.H., Miller, A.R., Vanoye, C.G., George, A.L., Kearney, J.A., 2014. Strain- and age-dependent hippocampal neuron sodium currents correlate with epilepsy severity in Dravet syndrome mice. Neurobiol. Dis. 65, 1–11.
Notenboom, R.G.E., Ramakers, G.M.J., Kamal, A., Spruijt, B.M., De Graan, P.N.E., 2010. Long-lasting modulation of synaptic plasticity in rat hippocampus after early-life complex febrile seizures. Eur. J. Neurosci. 32, 749–758.
Oakley, J.C., Kalume, F., Yu, F.H., Scheuer, T., Catterall, W.A., 2009. Temperature- and age-dependent seizures in a mouse model of severe myoclonic epilepsy in infancy. Proc. Natl. Acad. Sci. U. S. A. 106, 3994–3999.
Ogiwara, I., Miyamoto, H., Morita, N., Atapour, N., Mazaki, E., Inoue, I., Takeuchi, T., Itohara, S., Yanagawa, Y., Obata, K., et al., 2007. Nav1.1 localizes to axons of Parvalbumin-positive inhibitory interneurons: a circuit basis for epileptic seizures in mice carrying an Scn1a gene mutation. J. Neurosci. 27, 5903–5914.
Ogiwara, I., Iwasato, T., Miyamoto, H., Iwata, R., Yamagata, T., Mazaki, E., Yanagawa, Y., Tamamaki, N., Hensch, T.K., Itohara, S., et al., 2013. Nav1.1 haploinsufficiency in excitatory neurons ameliorates seizure-associated sudden death in a mouse model of Dravet syndrome. Hum. Mol. Genet. 22, 4784–4804.
Olivieri, G., Battaglia, D., Chieffo, D., Rubbino, R., Ranalli, D., Contaldo, I., Dravet, C., Mercuri, E., Guzzetta, F., 2016. Cognitive-behavioral profiles in teenagers with Dravet syndrome. Brain Dev. 38, 554–562.
Orsini, A., Zara, F., Striano, P., 2018. Recent advances in epilepsy genetics. Neurosci. Lett. 667, 4–9.
Parihar, R., Ganesh, S., 2013. The SCN1A gene variants and epileptic encephalopathies. J. Hum. Genet. 58, 573–580.
Patterson, J.L., Carapetian, S.A., Hageman, J.R., Kelley, K.R., 2013. Febrile Seizures. Pediatr. Ann. 42, e258–e263.
Purcell, R.H., Papale, L.A., Makinson, C.D., Sawyer, N.T., Schroeder, J.P., Escayg, A., Weinshenker, D., 2013. Effects of an epilepsy-causing mutation in the SCN1A sodium channel gene on cocaine-induced seizure susceptibility in mice. Psychopharmacology 228, 263–270 Berl.
Ragona, F., Granata, T., Dalla Bernardina, B., Offredi, F., Darra, F., Battaglia, D., Morbi, M., Brazzo, D., Cappelletti, S., Chieffo, D., et al., 2011. Cognitive development in Dravet syndrome: a retrospective, multicenter study of 26 patients. Epilepsia 52, 386–392.
Rubinstein, M., Westenbroek, R.E., Yu, F.H., Jones, C.J., Scheuer, T., Catterall, W.A., 2015. Genetic background modulates impaired excitability of inhibitory neurons in a mouse model of Dravet syndrome. Neurobiol. Dis. 73, 106–117.
Sawyer, N.T., Helvig, A.W., Makinson, C.D., Decker, M.J., Neigh, G.N., Escayg, A., 2016. Scn1a dysfunction alters behavior but not the effect of stress on seizure response. Genes Brain Behav. 15, 335–347.
Scheffer, I.E., Berkovic, S., Capovilla, G., Connolly, M.B., French, J., Guilhoto, L., Hirsch, E., Jain, S., Mathern, G.W., Moshé, S.L., et al., 2017. ILAE classification of the epilepsies: position paper of the ILAE commission for classification and terminology. Epilepsia 58, 512–521.
Stern, W.M., Sander, J.W., Rothwell, J.C., Sisodiya, S.M., 2017. Impaired intracortical inhibition demonstrated in vivo in people with Dravet syndrome. Neurology 88, 1659–1665.
Symonds, J.D., Zuberi, S.M., 2018. Genetics update: monogenetics, polygene disorders and the quest for modifying genes. Neuropharmacology 132, 3–19.
Tai, C., Abe, Y., Westenbroek, R.E., Scheuer, T., Catterall, W.A., 2014. Impaired excitability of somatostatin- and parvalbumin-expressing cortical interneurons in a mouse model of Dravet syndrome. Proc. Natl. Acad. Sci. U. S. A. 111, E3139–E3148.
Tao, K., Ichikawa, J., Matsuki, N., Ikegaya, Y., Koyama, R., 2016. Experimental febrile

seizures induce age-dependent structural plasticity and improve memory in mice. Neuroscience 318, 34–44.
Tsai, M.-L., Leung, L.S., 2006. Decrease of hippocampal GABA B receptor-mediated inhibition after hyperthermia-induced seizures in immature rats. Epilepsia 47, 277–287.
Tsai, M.-S., Lee, M.-L., Chang, C.-Y., Fan, H.-H., Yu, I.-S., Chen, Y.-T., You, J.-Y., Chen, C.-Y., Chang, F.-C., Hsiao, J.H., et al., 2015. Functional and structural deficits of the dentate gyrus network coincide with emerging spontaneous seizures in an Scn1a mutant Dravet Syndrome model during development. Neurobiol. Dis. 77, 35–48.
Verret, L., Mann, E.O., Hang, G.B., Barth, A.M.I., Cobos, I., Ho, K., Devidze, N., Masliah, E., Kreitzer, A.C., Mody, I., et al., 2012. Inhibitory interneuron deficit links altered network activity and cognitive dysfunction in Alzheimer model. Cell 149, 708–721.
Villeneuve, N., Laguitton, V., Viellard, M., Lepine, A., Chabrol, B., Dravet, C., Milh, M., 2014. Cognitive and adaptive evaluation of 21 consecutive patients with Dravet syndrome. Epilepsy Behav. 31, 143–148.
Wolff, M., Casse-Perrot, C., Dravet, C., 2006. Severe myoclonic epilepsy of infants (Dravet syndrome): natural history and neuropsychological findings. Epilepsia 47 (Suppl. 2), 45–48.
Yu, F.H., Mantegazza, M., Westenbroek, R.E., Robbins, C.A., Kalume, F., Burton, K.A., Spain, W.J., McKnight, G.S., Scheuer, T., Catterall, W.A., 2006. Reduced sodium current in GABAergic interneurons in a mouse model of severe myoclonic epilepsy in infancy. Nat. Neurosci. 9, 1142–1149.
Zhang, Y.-H., Burgess, R., Malone, J.P., Glubb, G.C., Helbig, K.L., Vadlamudi, L., Kivity, S., Afawi, Z., Bleasel, A., Grattan-Smith, P., et al., 2017. Genetic epilepsy with febrile seizures plus: refining the spectrum. Neurology 89, 1210–1219.